

Final Report of the O3M-SAF Activity:

Aerosol retrieval from GOME-2: Improving computational efficiency and first application

Otto Hasekamp^a, Olaf Tuinder^b, Piet Stammes^b

(a)SRON, Netherlands Institute for Space Research
Sorbonnelaan 2
3584 CA Utrecht, The Netherlands

(b)KNMI (Royal Netherlands Meteorological Institute)
P.O. Box 201, 3730 AE De Bilt, The Netherlands

Corresponding author: email O.Hasekamp@sron.nl, tel. +31 30 253 8563, fax +31 30 254 0860

Contents

1	Introduction	1
1.1	Background	1
1.2	This Report	2
2	GOME-2 and Polarization	5
2.1	Measurements of Polarization	5
2.1.1	Definitions for Intensity and Polarization	5
2.1.2	The GOME-2 instrument	5
3	Retrieval Algorithm based on Lookup-Tables	7
3.1	Retrieval Methodology	7
3.1.1	Lookup Tables for Aerosol Models	7
3.1.2	Retrievals over the Ocean	7
3.1.3	Retrievals over Land	9
3.1.4	Inversion Procedure	10
3.1.5	Cloud Filtering	11
3.2	Error Characterization	11
3.2.1	Aerosol Models	11
3.2.2	Instrument calibration errors	13
3.2.3	Height Distribution Errors	13
3.3	Summary and Conclusions	13
4	Retrieval of Aerosol Microphysical Properties: Full Physics Algorithm	15
4.1	Introduction	15
4.2	Retrieval Methodology	15
4.2.1	Forward model and Inversion	16
4.3	Levenberg-Marquardt iteration	17
4.4	Summary	17
5	Application to GOME-2 Data	19
5.1	Re-Calibration of Polarization data	19
5.2	Cloud Filtering	21
5.2.1	Retrievals over the ocean	21
5.2.2	Retrievals over land	23
5.3	Results LUT based algorithm	23
5.4	Results of Full Physics Algorithm	27

6	Conclusions & Outlook	35
6.1	Conclusions	35
6.1.1	LUT-Based Algorithm	35
6.1.2	Full Physics Algorithm	36
6.2	Outlook	36
	Bibliography	37

Chapter 1

Introduction

1.1 Background

Aerosols directly affect the Earth's climate by scattering incoming solar radiation back to space (cooling effect) and by absorbing long-wave radiation emitted by the Earth (warming effect). Aerosols also indirectly influence climate by changing the microphysical properties of clouds. The total aerosol effect represents one of the largest unknown factors in climate research. In order to improve our understanding of the effect of aerosols on climate, global measurements are needed of a number of aerosol properties such as aerosol size, refractive index and optical thickness. The only way to obtain these measurements at a global scale is by means of satellite remote sensing.

Many satellite instruments that are used for aerosol retrieval are multiple-wavelength single-viewing-angle instruments. Among these instruments are the Advanced Very High Resolution Radiometer (AVHRR), the Moderate Resolution Imaging Spectroradiometer (MODIS), the Total Ozone Mapping Spectrometer (TOMS), the Global Ozone Monitoring Experiment (GOME) and the Scanning Imaging Absorption Spectrometer for Atmospheric Chartography (SCIAMACHY). Although it has been shown that the aerosol optical thickness may be retrieved from these instruments [*Mishchenko et al.*, 1999; *Tanré et al.*, 1999; *Veefkind et al.*, 2000; *Torricella et al.*, 1999], the results depend critically on the assumed values of the other aerosol parameters (size distribution, refractive index). The aerosol information content of intensity measurements is significantly larger for instruments that perform measurements at multiple viewing angles, such as the Multiangle Imaging Spectro-Radiometer (MISR). However, the combined use of intensity and polarization measurements at multiple viewing angles have been shown to be most powerful for the purpose of aerosol retrieval [*Mishchenko and Travis*, 1997a, b; *Chowdhary et al.*, 2002, 2005]. The reason for this is the high sensitivity of polarization properties of light to aerosol microphysics [*Hansen and Travis*, 1974]. Multiple-viewing-angle satellite measurements of intensity and polarization in the spectral range 443-865 nm have been performed by the Polarization and Directionality of Earth's Reflectances-1 and -2 instruments (POLDER-1 and -2). Both instruments were active for about 8 months in 1996/1997 and 2002, respectively. Currently a POLDER-3 instrument is in orbit on the PARASOL satellite.

The GOME-2 instrument, launched in October 2006, measures intensity and polarization in one viewing direction. Due to the polarization measurements, the information content with respect to aerosol properties is significantly larger than for single viewing angle intensity measurements [*Mishchenko and Travis*, 1997a; *Hasekamp and Landgraf*, 2005b]. This makes GOME-2 an interesting instrument for GOME-2 retrieval. Two parallel algorithm developments are performed for GOME-2: (i) A computationally fast algorithm that is suited for operational processing, based on Lookup Tables (LUTs), and (ii) an algorithm for the retrieval of aerosol microphysical properties using an analytical inversion approach and online (vector) radiative transfer calculations. The latter algorithm is currently computationally too expensive for operational processing, and is intended to be used for scientific case studies.

1.2 This Report

This final report summarizes the Visiting Scientist activity on 'Aerosol retrieval from GOME-2: Improving computational efficiency and first application to GOME-2', carried out in the period April 2007-April 2008. This activity was a continuation of the VS activities on aerosol retrieval from GOME-2 conducted in the period 2003-2006. During the first VS project a detailed study has been performed on the possibilities for the retrieval of aerosol properties from GOME-2 measurements over the ocean. It was found that the intensity and polarization measurements performed by the Polarization Measuring Device (PMD) of GOME-2 are very suited for the retrieval of aerosol properties. An advantage of using the PMD measurements is that they allow the retrieval of detailed information on aerosol microphysical properties such as size distribution and refractive index. An additional advantage of using the PMD is that its ground pixel size is only 10x40 km², which is a factor 8 smaller than that of the main channels (80x40 km²). The smaller pixel size increases the number of cloud free scenes and leads to more homogeneous aerosol scenes.

Based on the feasibility study of the first VS project, in a next VS project a prototype algorithm has been developed for aerosol retrieval over the ocean from GOME-2 PMD measurements [Hasekamp and Landgraf, 2005a,b]. The developed algorithm uses an iterative retrieval approach, where in each iteration step a linearized radiative transfer model is fitted to the PMD measurements. The inversion is performed using the Philips-Tikhonov regularization method, which quantifies and extracts the available information on aerosol properties. All 8 parameters corresponding to a bi-modal aerosol model, and additionally the height of the aerosol layer, are considered as unknown. The algorithm has been successfully tested on synthetic GOME-2 measurements with realistic noise [Hasekamp and Landgraf, 2007].

In a recent VS project, the feasibility of aerosol retrieval over land surfaces has been investigated. It was found that in terms of information content the best option for aerosol retrieval over land is to use polarization measurements from the PMD together with main channel intensity measurements in the ultraviolet and the absorption bands of Oxygen. Namely, this set of measurements allows the simultaneous retrieval of aerosol properties and information on surface albedo. However, a disadvantage of this approach is that retrievals have to be performed at the spatial resolution of the main channels, which is significantly worse than that of the PMD. Another option for aerosol retrieval over land is to use only (PMD) measurements that are only little sensitive to surface reflection, i.e. intensity measurements in the ultraviolet and measurements of Stokes parameter Q for the full GOME-2 spectral range. For these retrievals more accurate a priori information on aerosol microphysical properties is required than for retrievals over the ocean that can use all PMD measurements.

As mentioned above, the algorithm developments of the previous VS activities were based on an iterative retrieval approach that requires online radiative transfer calculations including polarization. Such a retrieval approach is computationally expensive and will in the near future not be able to provide aerosol information for all cloud-free GOME-2 scenes. Therefore, the iterative algorithm can only be applied to a subset of the available cloud free PMD measurements. During the current VS activity we developed a simple and fast algorithm based on a lookup table (LUT) that can be applied to all cloud free PMD measurements. On one hand, such a LUT based algorithm allows us to provide a global aerosol optical thickness product on a short term. On the other hand, using the outcome of LUT based algorithm scenes can be identified for which it is interesting to obtain detailed information on aerosol properties from the iterative retrieval approach. The outcome of the LUT algorithm will then be used as first guess information for the iterative algorithm, which will reduce the number of iteration steps and thus speed up the iterative algorithm. Besides the development of the fast LUT based algorithm, we also adjusted the full iterative retrieval scheme such that it is able to process real GOME-2 data. Both the LUT based and the full iterative algorithm have been applied to real GOME-2 data. To obtain a stable retrieval with the full iterative retrieval, first the GOME-2 data needed to be re-calibrated.

Chapter 3 describes the LUT-based algorithm. This description has been adopted from the Algorithm Theoret-

ical Baseline Document (ATBD). Chapter 4 describes the adjustments made to the full iterative algorithm. Chapter 5 shows the first results of application of both algorithms to real GOME-2 data. Here, also the re-calibration procedure is discussed. Finally, the report is concluded in chapter 6.

Chapter 2

GOME-2 and Polarization

2.1 Measurements of Polarization

2.1.1 Definitions for Intensity and Polarization

The radiance and state of polarization of light at a given wavelength can be described by an intensity vector \mathbf{I} which has the Stokes parameters as its components *Chandrasekhar* [1960]:

$$\mathbf{I} = [I, Q, U, V]^T, \quad (2.1)$$

where T indicates the transposed vector, and the Stokes parameters are defined with respect to a certain reference plane. For multiple scattering calculations we will define the Stokes parameters relative to the local meridian plane, which is defined by the zenith direction and the direction of propagation of the light.

In terms of measurements, the Stokes parameters can be obtained in the following way [*Hansen and Travis*, 1974]:

$$\begin{aligned} I &= I(0^\circ, 0) + I(90^\circ, 0) = I_l + I_r \\ Q &= I(0^\circ, 0) - I(90^\circ, 0) = I_l - I_r \\ U &= I(45^\circ, 0) - I(135^\circ, 0) \\ V &= I(45^\circ, \pi) - I(135^\circ, \pi). \end{aligned} \quad (2.2)$$

So, I is the total intensity, Q is the difference in intensity of light transmitted by a polarizer which passes only light polarized parallel to the reference plane (I_l), and light transmitted by a polarizer which passes only light polarized perpendicular to the reference plane (I_r). Similarly, U is the difference in intensity transmitted by polarizers with $\Psi = 45^\circ$ and $\Psi = 135^\circ$, respectively. Stokes parameter V is the excess in intensity of light transmitted by an instrument that passes right handed polarization, over that transmitted by an instrument that passes left handed polarization. For scattering in the Earth atmosphere, V is negligibly small.

2.1.2 The GOME-2 instrument

GOME-2 is an improved version of GOME which aims to measure the global distribution of trace gases and aerosols. The main channels of GOME-2 measure the intensity reflected from the Earth atmosphere and surface in the spectral range 240-800 nm at a spectral resolution of 0.2-0.4 nm. The spatial resolution of the main channels is $80 \times 40 \text{ km}^2$. GOME-2 also contains a polarization measuring device (PMD) that measures I_l and I_r in 15 spectral bands in the range 300-800 nm, at a much better spatial resolution than the main channels, namely $10 \times 40 \text{ km}^2$. See Table 2.1 for the location of spectral bands of I_l and I_r . The GOME-2 polarization measurements are significantly improved compared to those of GOME and SCIAMACHY, both in spectral sampling and accuracy. The primary aim of the GOME-2 polarization measurements is to correct the main channel intensity measurements for

Table 2.1: Center of wavelength bands for PMD-l and PMD-r

Band nr.	Wavelength I_l [nm]	Wavelength I_r [nm]	FWHM [nm]
1	312.748	312.958	3.0
2	318.026	317.741	3.2
3	325.435	325.264	3.5
4	332.652	332.552	3.8
5	338.229	338.099	4.2
6	369.629	369.288	5.3
7	382.276	381.969	6.0
8	414.745	414.083	8.2
9	463.674	463.075	11.2
10	522.255	521.768	16.1
11	554.868	554.368	19.4
12	591.154	590.469	23.0
13	640.850	639.880	27.9
14	757.466	756.190	40.0
15	790.968	789.682	44.9

polarization sensitivity of the instrument. However, also important atmospheric information may be derived from these polarization measurements. Given the high sensitivity of polarization to aerosol microphysical properties, the GOME-2 PMD also offers an important opportunity for the retrieval of aerosol properties. *Mishchenko and Travis* [1997a] have shown that already at a single wavelength of 865 nm single-viewing-angle measurements of intensity together with polarization can provide important information. Considering also the spectral information, GOME-2 seems a promising candidate to provide a long time-series until about 2020 of important aerosol information.

Chapter 3

Retrieval Algorithm based on Lookup-Tables

3.1 Retrieval Methodology

3.1.1 Lookup Tables for Aerosol Models

In order to obtain a computationally efficient retrieval, radiative transfer calculations for different aerosol models (a combination of size distribution and refractive index), different values of the Aerosol Optical Thickness (AOT), and different surface reflection properties, were stored in Lookup Tables (LUTs). The aerosol models were adopted from the ATBD of the Ozone Monitoring Instrument (OMI) [Torres *et al.*, 2001]. These aerosol models contain 2 modes, where each mode is described by a log-normal function (see Appendix A). The aerosol models are summarized in Table 3.1. For the dust aerosol types (14-18) the imaginary part of the refractive index depends on wavelength, as depicted in Fig. 3.1. For aerosol models 1-18 all aerosols are uniformly distributed over the lowest 2 km of the atmosphere. Additionally, we constructed 11 more models with the same microphysical properties as models 8-18, but with all aerosols uniformly distributed between 4-6 km. These models represent elevated layers of biomass burning and dust aerosols.

The radiative transfer calculations were performed using a model based on the Gauss-Seidel iterative method [Landgraf *et al.*, 2001; Hasekamp and Landgraf, 2002]. The multiple scattering calculations were performed using 16 streams of a Double Gaussian Quadrature for the zenith angle dependence. The contribution of singly scattered light is computed separately. For all aerosol models the optical properties were calculated using Mie-theory [van de Hulst, 1957], thus assuming that particles are spherical. Concerning, the atmospheric profile, we used the US standard atmosphere of Anderson *et al.* [1987]

3.1.2 Retrievals over the Ocean

For retrievals over the ocean, the ocean reflection matrix can be described by three contributions (see e.g. [Chowdhary, 1999, and references therein]): 1) Fresnel reflection on the oceanic waves. This contribution is mainly determined by the wind speed W . 2) Scattering inside the ocean body called underlight. In this paper we restrict ourselves to the open ocean (so called 'case-1 waters' [Morel and Prieur, 1977]) for which the reflection due to underwater scattering is predominantly determined by the concentration of phytoplankton and its derivative products, referred to as the oceanic pigment concentration C_{pig} . 3) Reflection by oceanic foam, which depends on the foam albedo A_{fm} (see e.g. Frouin *et al.* [1996] and Kokhanovsky [2004]) and the fraction of the ground pixel that is covered by foam, which depends on the wind speed. So, the total ocean reflection depends mainly on the wind speed, the oceanic pigment concentration, and the foam albedo.

For the LUT calculations, the Fresnel reflection on the waves is calculated using the method of Mishchenko and Travis [1997a], assuming the wind speed dependent distribution of surface slopes proposed by Cox and Munk [1954]. For the foam albedo A_{fm} we assume a fixed value of 0.2. For the wind speed dependent fraction l_{fm} of the ground pixel that is covered by foam we use $l_{\text{fm}} = 2.95 \times 10^{-6} W^{3.52}$ [Monahan and O'Muircheartaigh, 1980].

Table 3.1: Center of wavelength bands for PMD-l and PMD-r

No.	r_{eff}^s	r_{eff}^l	v_{eff}^s	v_{eff}^l	f_l	m_r	m_i	type
1	0.11	0.84	0.65	0.65	$1.53 \cdot 10^{-2}$	1.40	$-5.0 \cdot 10^{-8}$	Oceanic
2	0.12	2.19	0.18	0.81	$4.36 \cdot 10^{-4}$	1.40	$-4.0 \cdot 10^{-3}$	Industrial
3	0.13	2.24	0.50	0.81	$4.04 \cdot 10^{-4}$	1.40	$-4.0 \cdot 10^{-3}$	Industrial
4	0.21	2.50	0.18	0.81	$8.10 \cdot 10^{-4}$	1.40	$-4.0 \cdot 10^{-3}$	Industrial
5	0.14	2.15	0.22	0.62	$7.00 \cdot 10^{-4}$	1.45	$-1.2 \cdot 10^{-2}$	Industrial
6	0.15	2.26	0.22	0.62	$6.84 \cdot 10^{-4}$	1.45	$-1.2 \cdot 10^{-2}$	Industrial
7	0.18	2.69	0.22	0.62	$6.95 \cdot 10^{-4}$	1.45	$-1.2 \cdot 10^{-2}$	Industrial
8	0.12	2.43	0.20	0.87	$1.70 \cdot 10^{-4}$	1.50	$-1.0 \cdot 10^{-2}$	Biomass
9	0.15	2.70	0.20	0.87	$2.06 \cdot 10^{-4}$	1.50	$-1.0 \cdot 10^{-2}$	Biomass
10	0.20	3.42	0.20	0.87	$2.94 \cdot 10^{-4}$	1.50	$-1.0 \cdot 10^{-2}$	Biomass
11	0.11	2.52	0.17	0.70	$2.07 \cdot 10^{-4}$	1.50	$-2.0 \cdot 10^{-2}$	Biomass
12	0.12	2.67	0.17	0.70	$2.05 \cdot 10^{-4}$	1.50	$-2.0 \cdot 10^{-2}$	Biomass
13	0.14	3.28	0.17	0.70	$1.99 \cdot 10^{-4}$	1.50	$-2.0 \cdot 10^{-2}$	Biomass
14-18	0.10	1.60	0.32	0.42	$4.35 \cdot 10^{-3}$	1.53	see Fig. 3.1	dust

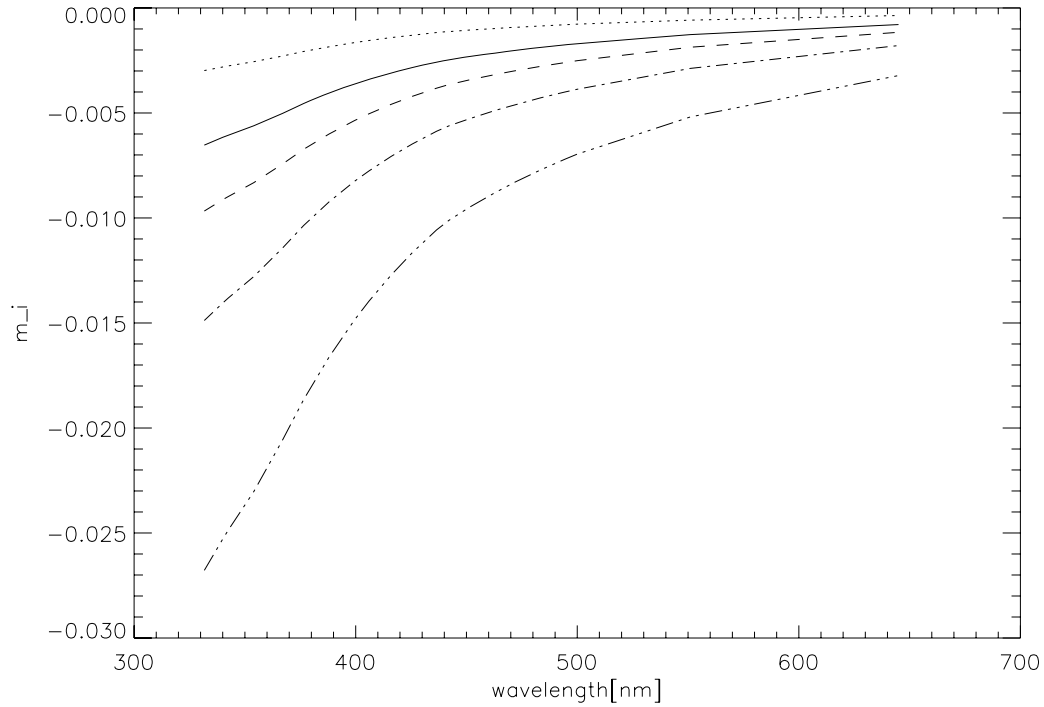


Figure 3.1: Imaginary part of refractive index for the five dust models. The spectra for models 14-18 are shown from top to bottom.

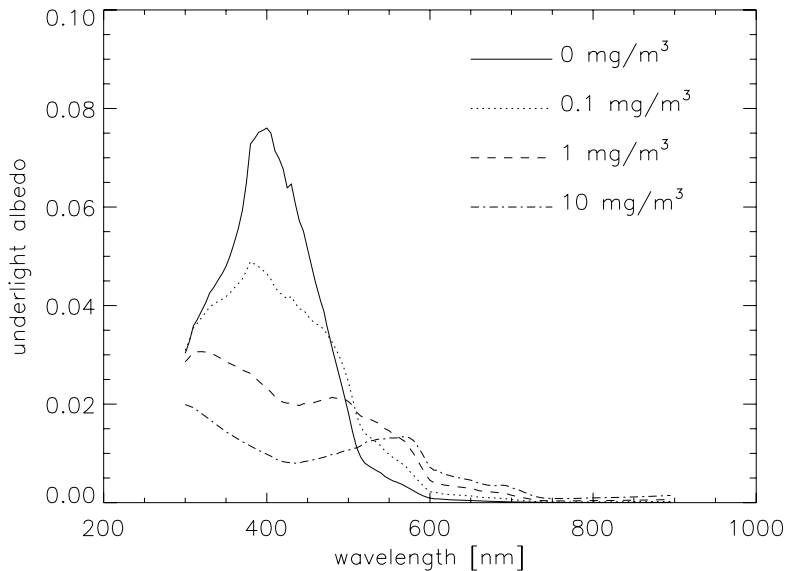


Figure 3.2: Oceanic underlight albedo as function of wavelength for different values of the oceanic pigment concentration.

The underlight contribution is described using a Lambertian albedo that depends on the oceanic pigment concentration, using the dependence given by *Morel* [1988] and *Morel and Gentili* [1993] in combination with the data of *Smith and Baker* [1981]. Figure 3.2 shows the Lambertian albedo as a function of wavelength for different oceanic pigment concentrations.

For aerosol retrieval over the ocean the 20 dimensional measurement vector \mathbf{y} contains the measured reflectance and Stokes fraction $q = Q/I$ in wavelength bands 6-15. Here, we use Stokes fraction q because it is measured with higher accuracy than Stokes parameter Q , because many errors cancel out in the determination of q , due to the similar optical paths for the l - and r PMDs [*Callies et al.*, 2000]. The 2 dimensional state vector \mathbf{x} contains the column integrated number density (directly related to the AOT) and the oceanic pigment concentration. The LUTs store radiative transfer calculations of Stokes parameter I and Stokes fraction q for wavelength band 6-15, for the 29 aerosol models. The values are stored as a function of aerosol optical thickness (550 nm), oceanic pigment concentration, windspeed, solar zenith angle, viewing zenith angle, relative azimuth angle. For the surface pressure a constant value of 1013 hPa has been used. See Table 3.2 for the different node points of the ocean LUT.

For one GOME-2 scene, the aerosol optical thickness and ocean pigment concentration are retrieved (see 3.1.4) for all aerosol models. Here, the windspeed is required as input from the ECMWF model.

3.1.3 Retrievals over Land

Over land surfaces the spectral dependence of the surface albedo in the range 350-800 nm cannot be characterized by a few parameters. Therefore, for aerosol retrieval over land we use a different approach than for aerosol retrieval over the ocean. First of all, we make use of the fact that the surface albedo is low and almost spectrally flat in the wavelength range 350-500 nm. Furthermore, we make use of the fact that Stokes parameter Q shows very low sensitivity to surface reflection. So, we define a 14-dimensional measurement vector that contains the measured

Table 3.2: Node points for LUT calculations for aerosol retrieval over the ocean

Variable name	unit	Nr. of entries	entries
aerosol optical thickness	[-]	8	0.1 0.3 0.5 0.8 1.0 2.0 3.0 4.0
aerosol models	[-]	29	1 2 ... 28 29
oceanic pigment concentrations	mg/m ³	5	10 ⁻⁵ 0.50 1.0 5.0 10.0
wind speed	m/s	3	3.0 7.0 11.0
surface pressure	hPa	1	1013
solar zenith angle	degrees	11	25.0 30.0 ... 70.0 75.0
viewing zenith angle	degrees	13	0.0 5.0 ... 55.0 60.0
cosine of azimuth angle	[-]	21	1.0 0.9 ... -0.9 -1.0

Table 3.3: Node points for LUT calculations for aerosol retrieval over land

Variable name	unit	Nr. of entries	entries
aerosol optical thickness	[-]	8	0.1 0.3 0.5 0.8 1.0 2.0 3.0 4.0
aerosol models	[-]	6	2, 5, 8, 12, 16, 19
surface albedo	[-]	9	0.00, 0.02, ..., 0.10, 0.15, 0.20, 0.80
surface pressure	hPa	2	700, 1013
solar zenith angle	degrees	11	25.0 30.0 ... 70.0 75.0
viewing zenith angle	degrees	13	0.0 5.0 ... 55.0 60.0
cosine of azimuth angle	[-]	21	1.0 0.9 ... -0.9 -1.0

reflectance in wavelength band 6-9 and measured sun-normalized Stokes parameter Q for wavelength band 6-15. From this measurement vector, a 2 dimensional state vector \mathbf{x} can be retrieved that contains the column integrated number density (directly related to the AOT) and a Lambertian surface albedo that is constant for PMD band 6-9 [Hasekamp, 2007]. Compared to retrievals over the ocean, this different measurement vector has a reduced information content with respect to aerosol properties, and is more sensitive to calibration errors (due to the use of Q instead of q). Due to the reduced information content for retrievals over land we reduced the number of aerosol models compared to the number of models for retrievals over the ocean. The node points of the LUT for aerosol retrieval over land are given in Table 3.3

3.1.4 Inversion Procedure

The first step in the inversion procedure is to interpolate the LUT values for a given aerosol model to the actual geometry, windspeed (for ocean), and surface pressure (for land). In this way we obtain tabulated values of a forward model \mathbf{F} that describes how the state vector \mathbf{x} and measurement vector \mathbf{y} are related,

$$\mathbf{y} = \mathbf{F}(\mathbf{x}) + \mathbf{e}, \quad (3.1)$$

where \mathbf{e} is an error term. To obtain values of \mathbf{F} in between the node points we use linear interpolation.

The forward model is non-linear in \mathbf{x} for variations in \mathbf{x} that are larger than the differences between the node points. Therefore, we solve the inversion problem iteratively, where in each iteration step we replace the forward model by it's linear approximation,

$$\mathbf{F}(\mathbf{x}_{n+1}) \approx \mathbf{F}(\mathbf{x}_n) + \mathbf{K} [\mathbf{x}_{n+1} - \mathbf{x}_n] \quad (3.2)$$

where \mathbf{x}_n is the state vector for the iteration step under consideration and \mathbf{K} is the Jacobian matrix containing the derivatives of the forward model with respect to the elements of \mathbf{x} . These derivatives are calculated numerically using the values of \mathbf{F} at the node points of the LUT.

The state vector for the next iteration step is obtained using the weighted least squares method.

$$\mathbf{x}_{n+1} = \min_{\mathbf{x}} \|\mathbf{S}_y^{-\frac{1}{2}}(\mathbf{K}\mathbf{x} - (\mathbf{y} - \mathbf{K}\mathbf{x}_n))\|^2 \quad (3.3)$$

$$= \mathbf{x}_n + (\mathbf{K}^T \mathbf{S}_y^{-1} \mathbf{K})^{-1} \mathbf{K}^T \mathbf{S}_y^{-1} (\mathbf{y} - \mathbf{K}\mathbf{x}_n) \quad (3.4)$$

where \mathbf{S}_y is the measurement error covariance matrix. The iteration is started with a state vector corresponding to the LUT node point for which the χ^2 difference between forward model and measurement is minimum. The iteration is continued until convergence has been reached.

The inversion procedure described above is performed for all aerosol models. The state vector for the aerosol model that yields, after convergence, the smallest χ^2 difference between forward model and measurement is selected as the retrieved state vector.

3.1.5 Cloud Filtering

It is intended to only perform aerosol retrievals for cloud free scenes. To identify whether a scene is contaminated with clouds, we use a quantity C_{clear} that expresses the contrast between the reflectivity (defined as $\pi I/\mu_o F_o$ where μ_o is the cosine of the solar zenith angle and F_o is the solar flux perpendicular to the solar beam) B measured in the 'blue' (~ 414 nm), the measured reflectivity G in the 'green' (~ 522 nm), and the reflectivity R in the 'red' (~ 640 nm) part of the spectrum [Krijger *et al.*, 2005]:

$$C_{\text{cloud}} = \frac{(\max(R, G, B) - \min(R, G, B).)}{\max(R, G, B)} \quad (3.5)$$

If C_{clear} exceeds a certain threshold the observed scene is considered cloud free. For this threshold value we chose 0.55.

We would like to note that cloud filtering is a critical issue for aerosol retrievals. Therefore, improvement of the cloud filtering procedure should be subject of further investigation

3.2 Error Characterization

3.2.1 Aerosol Models

Prior assumptions on the aerosol models can cause errors on the retrieved aerosol optical thickness. Here the most important source of error is due to the restriction to a limited number of aerosol models. If the correct aerosol model is not included in the set of pre-described models, the assumed aerosol phase function and single scattering albedo are not correct which will result in an error in the retrieved aerosol optical thickness. To investigate this source of error we constructed synthetic measurements for 1000 different atmospheric aerosol scenarios, where for each scenario we randomly chose the aerosol parameters within a specified range. This range was 0.1-0.2 μm for r_{eff} of the small mode, 0.17-0.65 for v_{eff} of the small mode, 0.8-3.4 μm for r_{eff} of the large mode, 0.5-0.9 for v_{eff} of the large mode, 1.3-1.7 for the real part of the refractive index, and $5 \cdot 10^{-7}$ -0.02 for the imaginary part of the refractive index. The aerosol column of both modes was chosen such that the corresponding aerosol optical thickness was between 0.01-0.25 at 550 nm. From these synthetic measurements we retrieved the aerosol optical thickness using the algorithm described here.

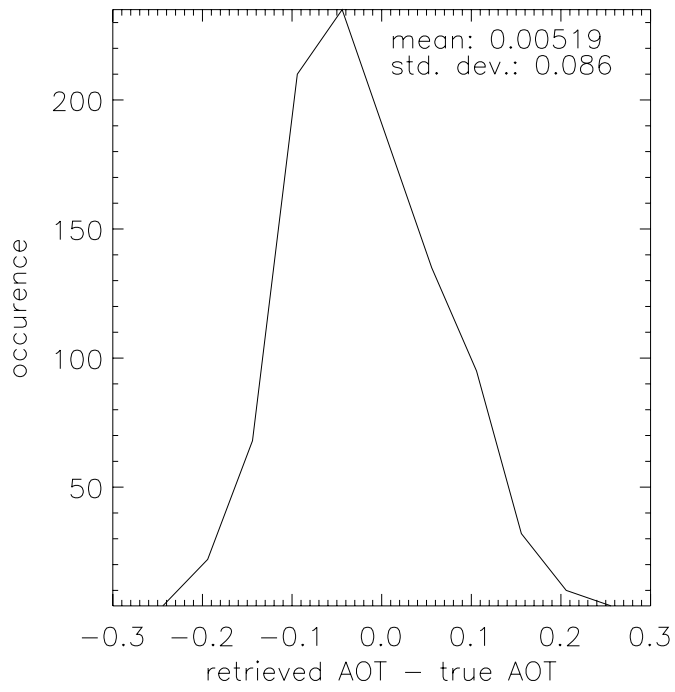


Figure 3.3: Histogram of the differences between the retrieved AOT and the true AOT for retrieval from synthetic measurements.

Figure 3.3 shows a histogram of the differences between the retrieved AOT and the true AOT. The mean difference is 0.005 whereas the standard deviation is 0.086. This can be considered as a rough estimate for the error in the retrieved AOT due to the restriction to a limited number of aerosol models.

3.2.2 Instrument calibration errors

The effect of instrument calibration errors on the retrieved AOT from GOME-2 has been reported by *Hasekamp and Landgraf* [2005b]. They studied the effect of three types of calibration errors: (i) a constant offset of 1%, (ii) an error of 1% in the first- and of -1% in the last PMD spectral band with a linear dependence on wavelength, and (iii) an error which is 1% at the first and last PMD spectral bands, -1% at the center wavelength and varies quadratically with wavelength. It was found that the a constant error of 1 % on the measured I and I_r causes an error on the retrieved AOT below 0.01. The effect of the linear error on the AOT is below 0.02, whereas the effect of the quadratic error is below 0.03.

3.2.3 Height Distribution Errors

The retrieval algorithm described here assumes that aerosols are uniformly distributed, either in a layer between 0-2 km or in a layer between 4-6 km. If in reality the aerosol number concentration decays with the 3rd power in pressure between up to 10 km, the error in the retrieved AOT is in the range 0.01-0.03 [*Hasekamp and Landgraf*, 2005b].

3.3 Summary and Conclusions

This document describes the algorithm for the retrieval of aerosol optical thickness from GOME-2 PMD measurements. The algorithm is based on Lookup Tables of radiative transfer calculations for different aerosol models, different values of the AOT, and different surface reflection properties.

For aerosol retrieval over the ocean the measurements of Stokes parameters I and Q of all 10 PMD spectral bands between 369-791 nm are used. The retrieved parameters are the aerosol column integrated number density (directly related to the AOT) and the oceanic pigment concentrations. For the retrieval 29 aerosol models are used, where the model that fits best to the measurement is selected.

For aerosol retrieval over land only measurements are used that show small sensitivity to surface reflection properties. These are the measurements of the intensity of the PMD bands in the range 369-463 nm, and measurements of Stokes parameter Q of the PMD bands in the range 369-791 nm. For these retrievals we retrieve the column integrated number density and a spectrally independent Lambertian surface albedo for the range 369-463 nm. The reduced measurement vector for retrievals over land has a smaller sensitivity to aerosol microphysical properties than the measurement vector for retrieval over the ocean. Therefore, for retrievals over land a limited number of 6 aerosol models is used.

Appendix A: Aerosol size distribution

We assume that the aerosol size distribution can be described as a bimodal distribution:

$$n(r) = (1 - f_c) n_s(r) + f_c n_c(r), \quad (3.6)$$

where r is particle radius, f_c is the coarse mode particle fraction, and n_s and n_c are the size distribution of the small and coarse mode, respectively. We assume that n_s and n_c can be described by a log-normal function n_{\ln} :

$$n_{\ln}(r) = \frac{1}{\sqrt{2\pi} \sigma_g r} \exp [-(\ln r - \ln r_g)^2 / (2\sigma_g^2)], \quad (3.7)$$

where

$$\ln r_g = \int_0^{\infty} \ln r n(r) dr, \quad (3.8)$$

and

$$\sigma_g^2 = \int_0^{\infty} (\ln r - \ln r_g)^2 n(r) dr. \quad (3.9)$$

As shown by Hansen and Travis *Hansen and Travis* [1974] it is useful to characterize (a mode of) the size distribution by the effective radius r_{eff} and effective variance v_{eff} , because these parameters are relatively independent from the actual shape of the distribution. Here,

$$r_{\text{eff}} = \frac{1}{G} \int_0^{\infty} r \pi r^2 n(r) dr, \quad (3.10)$$

and

$$v_{\text{eff}} = \frac{1}{Gr_{\text{eff}}^2} \int_0^{\infty} (r - r_{\text{eff}})^2 \pi r^2 n(r) dr, \quad (3.11)$$

where G is the geometrical cross section. We use the superscripts l and s to refer to the small and large mode of the size distribution, respectively.

The relation between r_{eff} , v_{eff} on one hand, and r_g and σ_g on the other hand is given by:

$$\begin{aligned} r_g &= r_{\text{eff}} / (1 + v_{\text{eff}})^{5/2} \\ \sigma_g^2 &= \ln(1 + v_{\text{eff}}). \end{aligned} \quad (3.12)$$

Chapter 4

Retrieval of Aerosol Microphysical Properties: Full Physics Algorithm

4.1 Introduction

In chapter 3 we described a retrieval algorithm that is based on fitting tabulated radiative transfer calculations for a limited number of standard aerosol models to the GOME-2 measurements of intensity and polarization. An advantage of such an approach is that it is computationally fast enough to process (and re-process) large amounts of GOME-2 data. A disadvantage is that in reality aerosols cannot be described by a limited number of models. Here, errors in the assumed aerosol models may cause significant errors on the retrieved aerosol optical thickness (see Fig. 3.3 in chapter 3). Furthermore, a LUT based retrieval approach does not make full use of the increased information content of combined intensity and polarization measurements compared to instruments that measure only intensity. Namely, the additional use of GOME-2 polarization measurements allows the retrieval of information on size distribution and refractive index, which are essential parameters for climate research. In the paper of *Hasekamp and Landgraf* [2005b] a retrieval method is described that makes full use of the retrieval capabilities of GOME-2. In order to apply this approach to real data some adjustments of the algorithm had to be made. This chapter describes the revised algorithm for the retrieval of aerosol microphysical properties from GOME-2. Here, we restrict ourselves to retrieval of aerosol properties over the ocean, where the information content is largest.

4.2 Retrieval Methodology

We assume that the aerosol size distribution can be described by a bi-modal log normal function, where each mode is characterized by the effective radius r_{eff} , the effective variance v_{eff} (see Appendix B) and the column integrated aerosol number concentration N . In what follows we use the superscripts l and s to refer to the small and large mode of the size distribution, respectively. Additionally, the complex refractive index $m = m_r + im_i$ is needed to characterize aerosols. Furthermore, we assume that aerosols are uniformly distributed over an altitude layer of 2 km thickness.

In the setup described above there are 9 unknown aerosol parameters. These are the effective radius r_{eff} of the small- and large mode, the effective variance v_{eff} of the small- and large mode, the column integrated aerosol number concentration N of the small- and large mode, the real- and imaginary part of the refractive index, and the height of the aerosol layer.

In addition to the scattering and absorption properties of the atmosphere, the satellite measurement is also affected by the reflection properties of the ocean. The ocean reflection can be described by three contributions (see e.g. [*Chowdhary*, 1999, and references therein]): 1) Fresnel reflection on the oceanic waves. This contribution is mainly determined by the wind speed W . 2) Scattering inside the ocean body called underlight. In this paper we restrict ourselves to the open ocean (so called 'case-1 waters' [*Morel and Prieur*, 1977]) for which the reflection

due to underwater scattering is predominantly determined by the concentration of phytoplankton and its derivative products, referred to as the oceanic pigment concentration C_{pig} . 3) Reflection by oceanic foam, which depends on the foam albedo A_{fm} (see e.g. *Frouin et al.* [1996] and *Kokhanovsky* [2004]) and the fraction of the ground pixel that is covered by foam, which depends on turn on the wind speed. So, the total ocean reflection depends mainly on the wind speed, the oceanic pigment concentration, and the foam albedo. Of these parameters we include the oceanic pigment concentration as an additional unknown parameter in our retrieval. Furthermore, we assume the wind speed is accurately known from a meteorological model and we use a fixed foam albedo.

4.2.1 Forward model and Inversion

Let us now define a state vector \mathbf{x} that contains the parameters to be retrieved, i.e. the 9 aerosol parameters and the oceanic pigment concentration as an additional parameter. Furthermore, let us define a measurement vector \mathbf{y} that contains the satellite measurements of Stokes parameters I and Q in different spectral bands. The retrieval of state vector \mathbf{x} from measurement vector \mathbf{y} requires a forward model \mathbf{F} that describes how \mathbf{y} and \mathbf{x} are related, viz.

$$\mathbf{y} = \mathbf{F}(\mathbf{x}) + \mathbf{e}_y, \quad (4.1)$$

where \mathbf{e}_y is an error term. The forward model consists of two parts. The first part relates the physical aerosol properties (size distribution, refractive index) to their optical properties (optical thickness, single scattering albedo, phase matrix). This relation can be described by Mie theory for spherical particles [*van de Hulst*, 1957] or alternative theories for particles with other shapes (see e.g. *Kokhanovsky* [2003]; *Wiscombe and Grams* [1988]; *Koepke and Hess* [1988]; *Mishchenko and Travis* [1994]; *Mishchenko et al.* [1995]). In this paper we only consider spherical aerosols which allows the use of Mie theory. The second part of the forward model is an atmospheric radiative transfer model that simulates the intensity vector at the top of the atmosphere for given optical input parameters. Here, we use the vector radiative transfer model described by *Hasekamp and Landgraf* [2002] and *Hasekamp and Landgraf* [2005a], to model the transport of radiation in the atmosphere. This model solves the radiative transfer equation using the Gauss-Seidel iterative method.

The aim of an inversion algorithm is to find a state vector $\hat{\mathbf{x}}$ for which forward model $\mathbf{F}(\hat{\mathbf{x}})$ and measurement \mathbf{y} are in optimal agreement. Since the forward model is not linear in the unknown parameters the solution of the inversion problem has to be found iteratively. Here, we replace for each iteration step n the forward model in (4.1) by its linear approximation,

$$\mathbf{F}(\mathbf{x}_{n+1}) \approx \mathbf{F}(\mathbf{x}_n) + \mathbf{K} [\mathbf{x}_{n+1} - \mathbf{x}_n] \quad (4.2)$$

where \mathbf{x}_n is the state vector for the iteration step under consideration and \mathbf{K} is the Jacobian matrix containing the derivatives of the forward model with respect to the elements of \mathbf{x}_n , where element K_{ij} of \mathbf{K} is defined by:

$$K_{ij} = \frac{\partial F_i}{\partial x_j}(\mathbf{x}_n). \quad (4.3)$$

The satellite measurements considered here do not contain sufficient information to retrieve all 10 unknown parameters, and thus the corresponding inverse problem is ill-posed. This means that many combinations of the 10 parameters fit the measurement almost equally well. As a result, the least-squares solution $\hat{\mathbf{x}}_{\text{lsq}}$ to our retrieval problem, viz.

$$\hat{\mathbf{x}}_{\text{lsq}} = \min_{\mathbf{x}} \|\mathbf{S}_y^{-\frac{1}{2}}(\mathbf{F}(\mathbf{x}) - \mathbf{y})\|^2, \quad (4.4)$$

is overwhelmed by noise. In order to obtain a stable inversion, we introduce a reduced state vector \mathbf{x}_{red} that only contains a the following subset of aerosol parameters: the height integrated aerosol number concentration of both modes, the effective radius of the small mode, the real part of refractive index, and the oceanic pigment

concentration. It is confirmed by the study of *Hasekamp and Landgraf* [2005b] that GOME-2 measurements are most sensitive to this subset of parameters. The other parameters are kept fixed at the values from the standard model that has been selected by the LUT algorithm. For each iteration step the least squares solution for \mathbf{x}_{red} is given by

$$\mathbf{x}_{\text{red},n} = \mathbf{x}_{\text{red},n-1} + (\mathbf{K}_{\text{red}}^T \mathbf{S}_y^{-1} \mathbf{K}_{\text{red}})^{-1} \mathbf{K}_{\text{red}}^T \mathbf{S}_y^{-1} (\mathbf{y} - \mathbf{F}(\mathbf{x}_{\text{red},n-1})), \quad (4.5)$$

where \mathbf{K}_{red} is the Jacobian matrix for the reduced state vector. The error covariance matrix of the solution is given by

$$\mathbf{S}_x = (\mathbf{K}_{\text{red}}^T \mathbf{S}_y^{-1} \mathbf{K}_{\text{red}})^{-1}. \quad (4.6)$$

4.3 Levenberg-Marquardt iteration

In general, the inversion of Eq. (4.1) represents a highly non-linear problem. Therefore, if the first guess state vector \mathbf{x}_o is too far from the true state vector the linear approximation in Eq. (4.2) may be poor. In that case, the inversion of the linearized forward model in Eq. (4.2) may result in a new state vector that yields a higher χ^2 difference between forward model $\mathbf{F}(\mathbf{x}_{n+1})$ and measurement \mathbf{y} than the first guess state vector \mathbf{x}_o , i.e. a step has been taken in the wrong direction. In order to prevent the inversion from taking a large step away from the minimum χ^2 , we use the Levenberg-Marquardt method [*Levenberg*, 1944; *Marquardt*, 1963], which minimizes the step size between two iteration steps in addition to minimizing the difference between linearized forward model and measurement.

Extensive tests of the iteration scheme have been reported in *Hasekamp and Landgraf* [2005a] and *Hasekamp and Landgraf* [2007].

4.4 Summary

This chapter describes an algorithm for the retrieval of aerosol microphysical properties from GOME-2 measurements over the ocean. The following parameters of a bi-modal aerosol model are retrieved: the height integrated aerosol number concentration of both modes, the effective radius of the small mode, the real part of refractive index, and the oceanic pigment concentration. It is confirmed by the study of *Hasekamp and Landgraf* [2005b] that GOME-2 measurements are most sensitive to this subset of parameters. These parameters are retrieved by least square fitting of a radiative transfer model to the GOME-2 measurements. In order to treat non-linearity we employ the Levenberg-Marquardt method [*Levenberg*, 1944; *Marquardt*, 1963]. For a sensitivity study and error analysis concerning the retrieval of microphysical properties, we refer to the paper of *Hasekamp and Landgraf* [2005b] and the O3MSAF Visiting Scientist report of *Hasekamp et al.* [2004]; *Hasekamp* [2005].

Chapter 5

Application to GOME-2 Data

5.1 Re-Calibration of Polarization data

For certain observed scenes along an orbit the viewing geometry is such that Stokes fraction $q = 0$, regardless of the observed atmosphere and surface [Aben *et al.*, 2003]. Namely, we can write

$$q = Q/I = P \cos 2\chi \quad (5.1)$$

$$u = U/I = P \sin 2\chi, \quad (5.2)$$

where P is the degree of linear polarization and χ is the direction of polarization relative to the local meridian plane. From Eq. (5.2) it follows that if $\chi = 45^\circ$ or 135° , then Stokes parameters $q = 0$. So, the geometries for which $\chi = 45^\circ$ can be used for validation of the level-1 data of Stokes fraction q .

Figure 5.1 shows Stokes fraction q as a function of viewing zenith angle (VZA) for geometries for which $\chi = 45^\circ$ or 135° . It can be seen that q is in the range 0-0.05 for most values of the VZA. The deviation from zero strongly depends on VZA. In order for polarization measurements to be useful for aerosol retrieval the accuracy should be better than 0.01. So, Fig. 5.1 clearly shows that the current calibration is not accurate enough. Therefore, we propose to adapt the calibration such that $q = 0$ for the geometries of Fig. 5.1. This has been done as described below.

At geometries for which $q = 0$, the intensities measured by the l and r PMDs should be equal (See Eq. (2.3), viz.

$$I_l = I_r \quad \text{if } \cos 2\chi = 0. \quad (5.3)$$

Therefore, we apply correction factors C_l and C_r to I_l and I_r , respectively, in order to obtain corrected values I_l^{corr} and I_r^{corr} , such that Eq. (5.3) is satisfied:

$$I_l^{corr} = C_l I_l I_r^{corr} = C_r I_r. \quad (5.4)$$

Of course, Eq. (5.3) does not uniquely determine the two correction factors. Namely, it is not known what the true intensity is to which both I_l and I_r should be corrected to. We have chose to consider the average between I_l and I_r as the true value. This yields correction factors

$$\begin{aligned} C_l &= \frac{(I_l + I_r)}{2I_l} & \text{if } \cos 2\chi = 0. \\ C_r &= \frac{(I_l + I_r)}{2I_r}. & \text{if } \cos 2\chi = 0. \end{aligned} \quad (5.5)$$

These correction factors are then determined for different values of the VZA, where all measurements corresponding to one VZA are averaged. The correction factor (5.5 ensure that Stokes fraction q is as close as possible to zero at the specific geometries, but the the choice to consider $\frac{(I_l+I_r)}{2}$ as the true value is an arbitrary choice. Therefore, we expect that the calibration of the Stokes fraction q has been improved considerably by applying C_l and C_r , but not the calibration of the total intensity $I = I_l + I_r$.

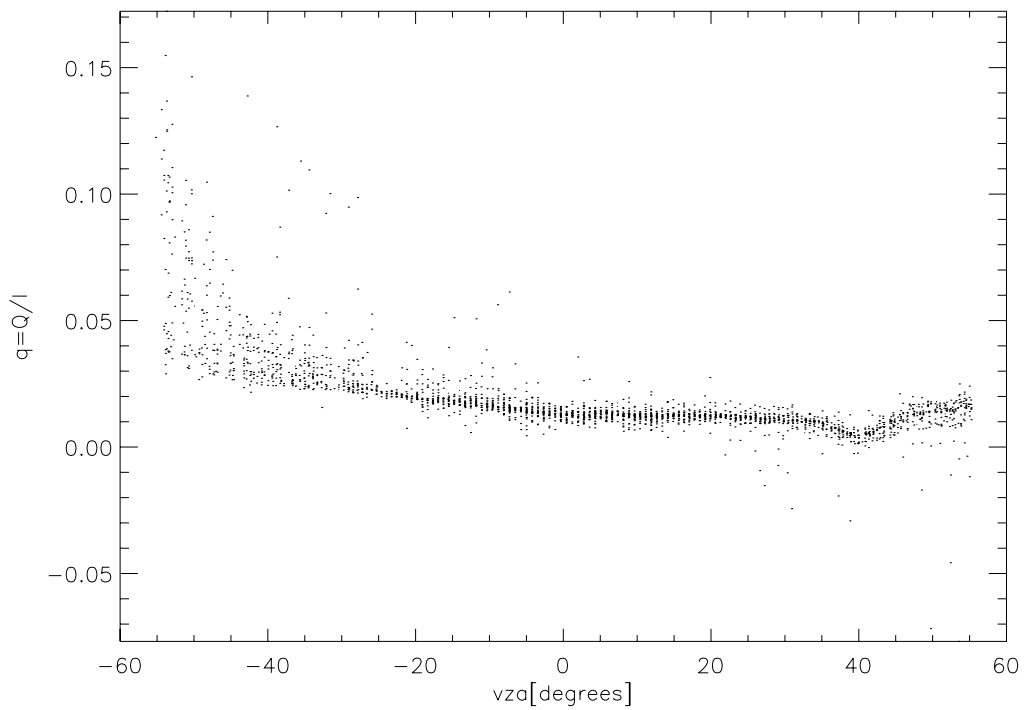


Figure 5.1: Measured Stokes fraction q as a function of VZA for geometries for which $\chi = 45^\circ$ or 135° . All GOME-2 level 1b data (version 3.9) of 2008-02-05 have been used

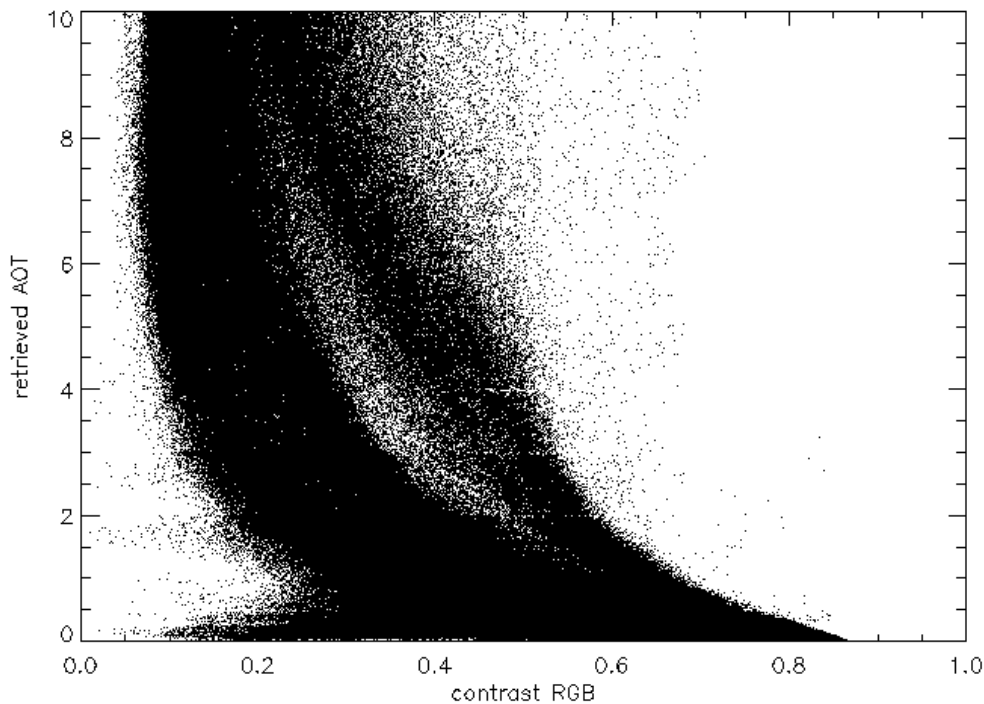


Figure 5.2: Retrieved AOT (550 nm) versus spectral contrast when no cloud filtering is applied. Results over the ocean.

5.2 Cloud Filtering

5.2.1 Retrievals over the ocean

It is intended to only perform aerosol retrievals for cloud free scenes. To identify whether a scene is contaminated with clouds, we use a filter based on the spectral contrast as defined in Eq. (3.5). To investigate the relation between the contrast C_{cloud} and cloudiness, we performed retrievals of the AOT for one day without cloud filtering, i.e. for all measurements of one day. Figure 5.2 shows the retrieved AOT versus the spectral contrast C_{cloud} . For retrievals over the ocean it can be seen that for small spectral contrast more retrievals yield a large value for the AOT, which is expected if an aerosol retrieval is performed in the presence of clouds. The selection of a threshold value for C_{cloud} is rather arbitrary. We have chosen a value of $C_{\text{cloud}} = 0.6$, as just below this value the retrieved AOT increases strongly for part of the scenes. Clearly, a cloud filter based on only the spectral contrast will also filter out aerosol scenes with small spectral contrast. Therefore, we also use a second check for cloud contamination based on the value of the reflectivity in the red part of the spectrum. If the value R of the reflectivity in the red (640 nm) is smaller than 0.10, the scene is considered cloud free independent of the spectral contrast. To motivate this Fig. 5.3 shows the retrieved AOT versus the spectral contrast C_{cloud} for scenes with $R < 0.10$. It can clearly be seen that the large values of the retrieved AOT disappeared. If a larger value than 0.1 is chosen part of the branches of Fig. 5.2 become visible again. Therefore, for aerosol retrievals over the ocean we select a scene as cloud-free if either $C_{\text{cloud}} > 0.60$ or $R < 0.10$.

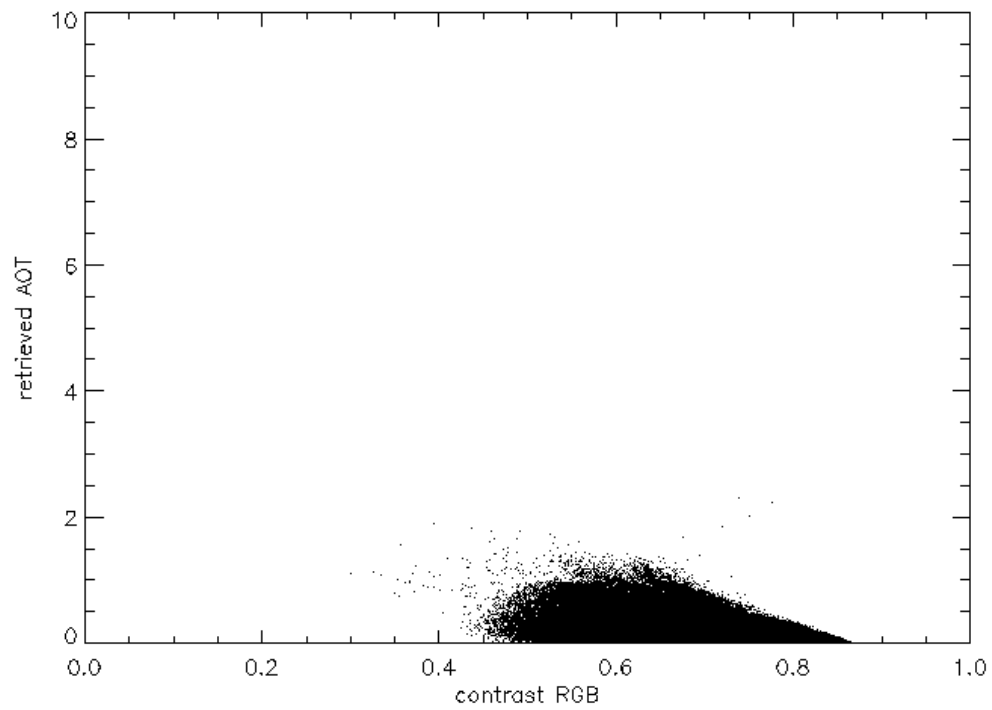


Figure 5.3: Retrieved AOT (550 nm) versus spectral. Only data are included with a reflectivity in the red part (640 nm) of the spectrum $R < 0.1$. Results over the ocean.

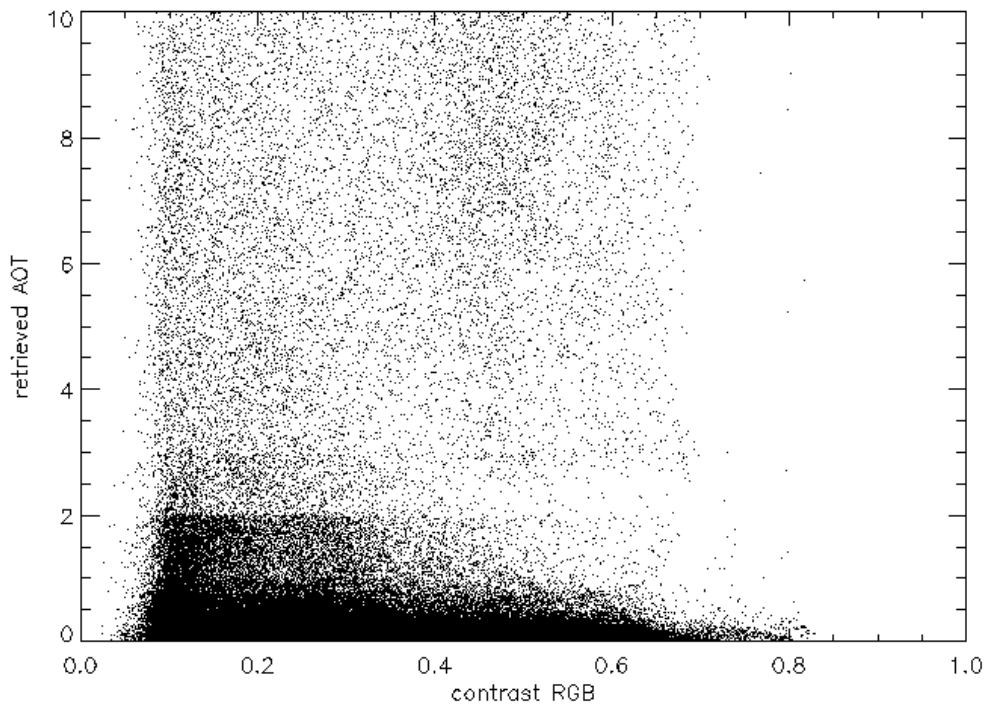


Figure 5.4: Retrieved AOT versus spectral contrast when no cloud filtering is applied. Results over land.

5.2.2 Retrievals over land

Figure 5.4 shows the retrieved AOT versus C_{cloud} for retrievals over land. The relationship is much less clear than for retrievals over the ocean. This is due to the effect that over land much of the spectral contrast can be caused by surface reflectance. Therefore, over land surface we select cloud free scenes based on a reflectivity criterion only. Here, we use the reflectivity B in the blue part (440 nm) of the spectrum because this value is less affected by surface reflection than the reflectivity in the green or red part of the spectrum. We consider scenes with $B < 0.30$ as cloud-free. Fig. 5.5 shows the retrieved AOT versus the spectral contrast C_{cloud} for scenes with $B < 0.30$. It can be seen that much less retrievals yield an unrealistic large AOT for this cloud filter.

5.3 Results LUT based algorithm

Figure 5.6 shows the retrieved AOT for 2008-02-05 for all scenes that are selected as cloud free by the cloud filter. In general, over the ocean the AOT is in the range that is expected for the AOT (0.1-0.3 for most scenes). Also some regions with higher AOT are present near the east and west coast of Africa, which might be explained by dust storms and/or biomass burning, and in Asia, which might be related to industrial pollution. The mean AOT over the ocean is 0.33 which is somewhat high. A possible explanation for this is that the cloud filter is not properly working, i.e. it flags some partly cloudy pixels as cloud free which results in a too high AOT. Furthermore, a significant error in the AOT is introduced due to the retrieval approach based on a limited number of aerosol types (see Fig. 3.3). Over land it seems that too many pixels are flagged as (partly) cloudy by the cloud filter, because the AOT is retrieved only for a small fraction of the scenes over land. For the scenes where the AOT is retrieved, the values are roughly in the range that may be expected.

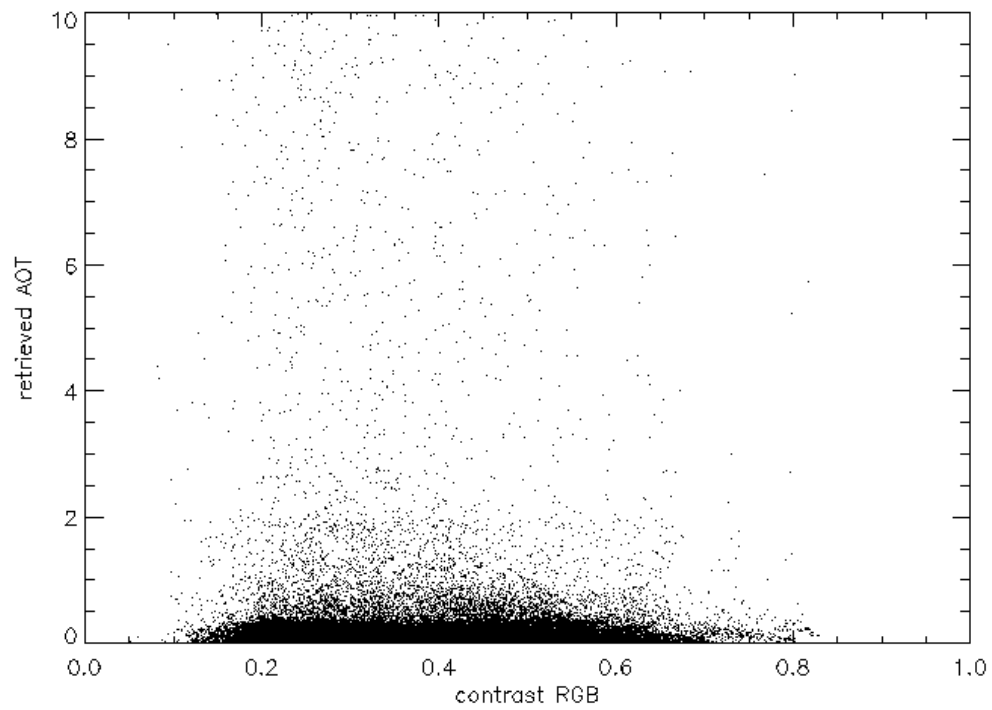


Figure 5.5: Retrieved AOT versus spectral contrast when no cloud filtering is applied. Only data are included with a reflectivity in the blue (440 nm) part of the spectrum $B < 0.3$. Results over land.

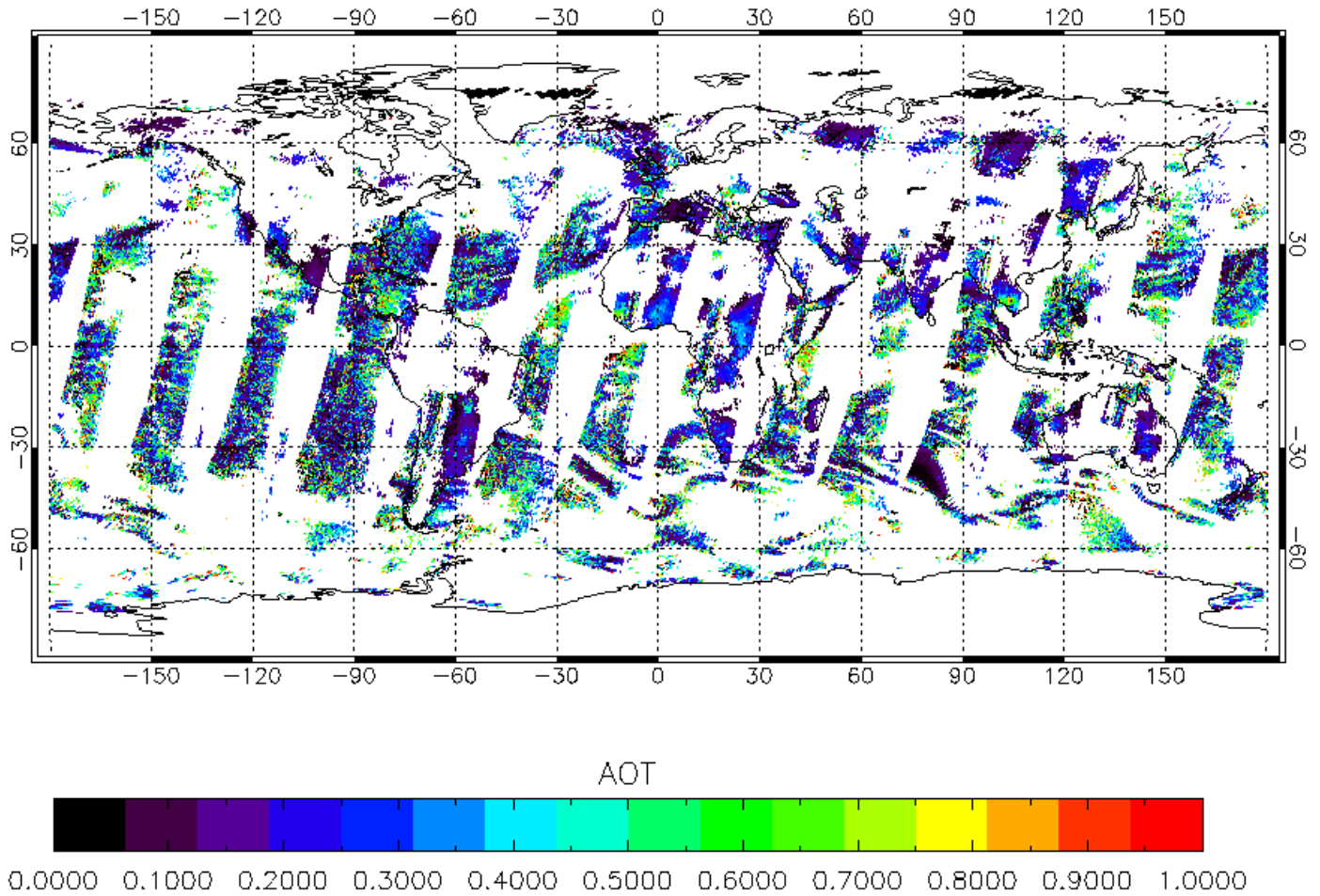


Figure 5.6: Retrieved AOT from GOME-2 for 2008-02-05 for all scenes that are selected as cloud-free

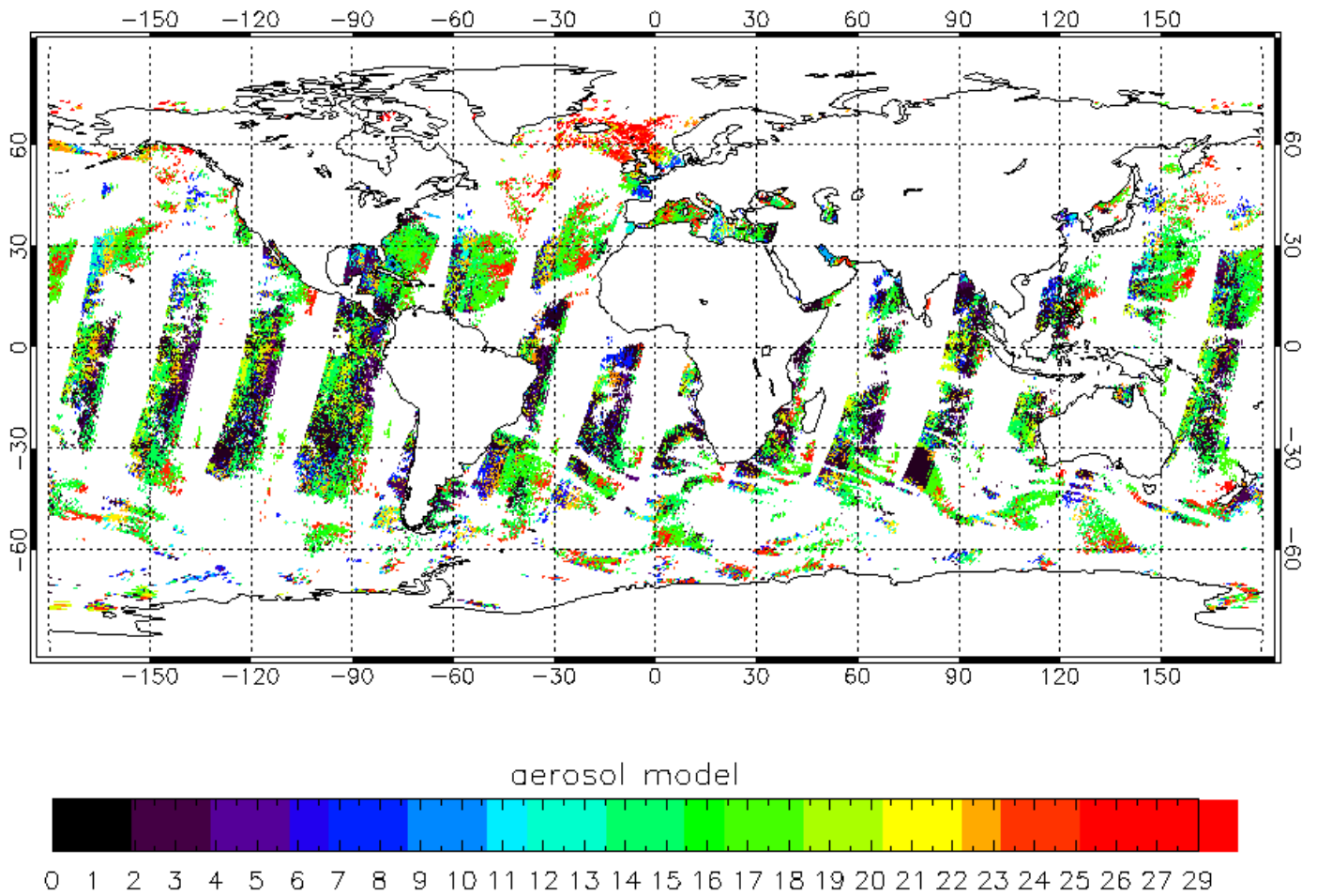


Figure 5.7: Aerosol models for 2008-02-05 for all scenes over the ocean that are selected as cloud-free

Figure 5.7 shows the aerosol models that yield the best fit to the measurements for all (assumed) cloud-free scenes over the ocean. A remarkable feature is that aerosol model 15 (dust) is the model that is selected for the majority of the scenes. It is not very likely that these scenes really correspond to dust events. In fact, it would be more realistic if the oceanic aerosol type (model 1) would have been selected for the majority of the cases. A possible explanation is that the aerosol model parameters of model 1 do not represent oceanic aerosols well, and that this type of aerosols is better represented by model 15, which is also dominated by large particles (which is expected over the unpolluted ocean). Another problem with the 'retrieved' aerosol models is that there appears to be a dependence on viewing geometry. This may be explained by the fact that the sensitivity of the GOME-2 polarization measurements to aerosol microphysical properties depends on geometry [Hasekamp and Landgraf, 2005b]. So, if the real microphysical properties are somewhere in between the values of two models, it may depend on viewing geometry which model fits best to the measurement. For example, at some geometries the measurement might be more sensitive to refractive index and the model will be selected of which the refractive index is close to the true value, while at other geometries the measurement might be more sensitive to effective radius. These problems are inherent to the retrieval approach based on a limited number of aerosol models.

Figure 5.8 shows the retrieved chlorophyll concentration (ocean) and UV surface albedo for 20080205. In general the values over the open ocean are in the range that is expected [Chowdhary *et al.*, 2001], but also scenes are present with a slightly negative chlorophyll concentration. This may be due to the simplified model for underwater scattering that has been used, or it may hint at calibration errors. It is important to note that the model used to describe underwater scattering are less suited for coastal waters, which makes the results there hard to interpret. The retrieved UV surface albedo over land is mostly (except for outliers at high latitudes) between 0.01 and 0.1, which is in the range that may be expected.

Figure 5.9 shows the retrieved AOT for 2008-04-01. Also for this day the values over the ocean are roughly in the range that is expected. Enhanced values of the AOT are present over the ocean west of the Sahara. For comparison, we show in Fig. 5.10 the aerosol absorption index [de Graaf *et al.*, 2005] deduced from GOME-2 data of the same day. The aerosol absorption index is a quantity that is sensitive to elevated layers of absorbing aerosols, such as desert dust. Also in the aerosol absorption index the dust plume west of the Sahara is visible. At other parts of the globe the enhanced values of the retrieved AOT (e.g. around Asia) are not confirmed by the aerosol absorption index. This may well be due to the fact that the aerosol absorption index is only sensitive to absorbing aerosols at high altitudes, while the enhanced values of the retrieved AOT may be due to non-absorbing aerosols in the boundary layer.

Over land the values appear to be too high and the results show unrealistic land-sea boundaries. Also, clear differences are seen between overlapping orbits. Clearly, the retrievals over land are subject to large uncertainties. This is caused (among other reasons) by the smaller information content caused by the reduced spectral range, the assumption that the surface is a Lambertian reflector, the stronger dependence on absolute calibration (not Stokes fraction q is used but Stokes parameter Q).

5.4 Results of Full Physics Algorithm

Because of the large amount of computational effort required, the Full Physics algorithm has only been applied to a small subset of the data. Figures 5.11 and 5.12 show respectively the AOT of the small and large mode, the effective radius of the small mode, and the refractive index retrieved on 2008-02-05 near the coast of Florida and Middle America. Both the AOTs as well as the effective radius and refractive index are in a physically realistic range. Between Cuba and middle America enhanced values of the AOT (especially the small mode) are seen. It is interesting that the retrieved effective radius of the small mode has smaller values in this region than in other regions of the figure. This may be an indication of the presence of anthropogenic aerosols. Also the retrieved refractive

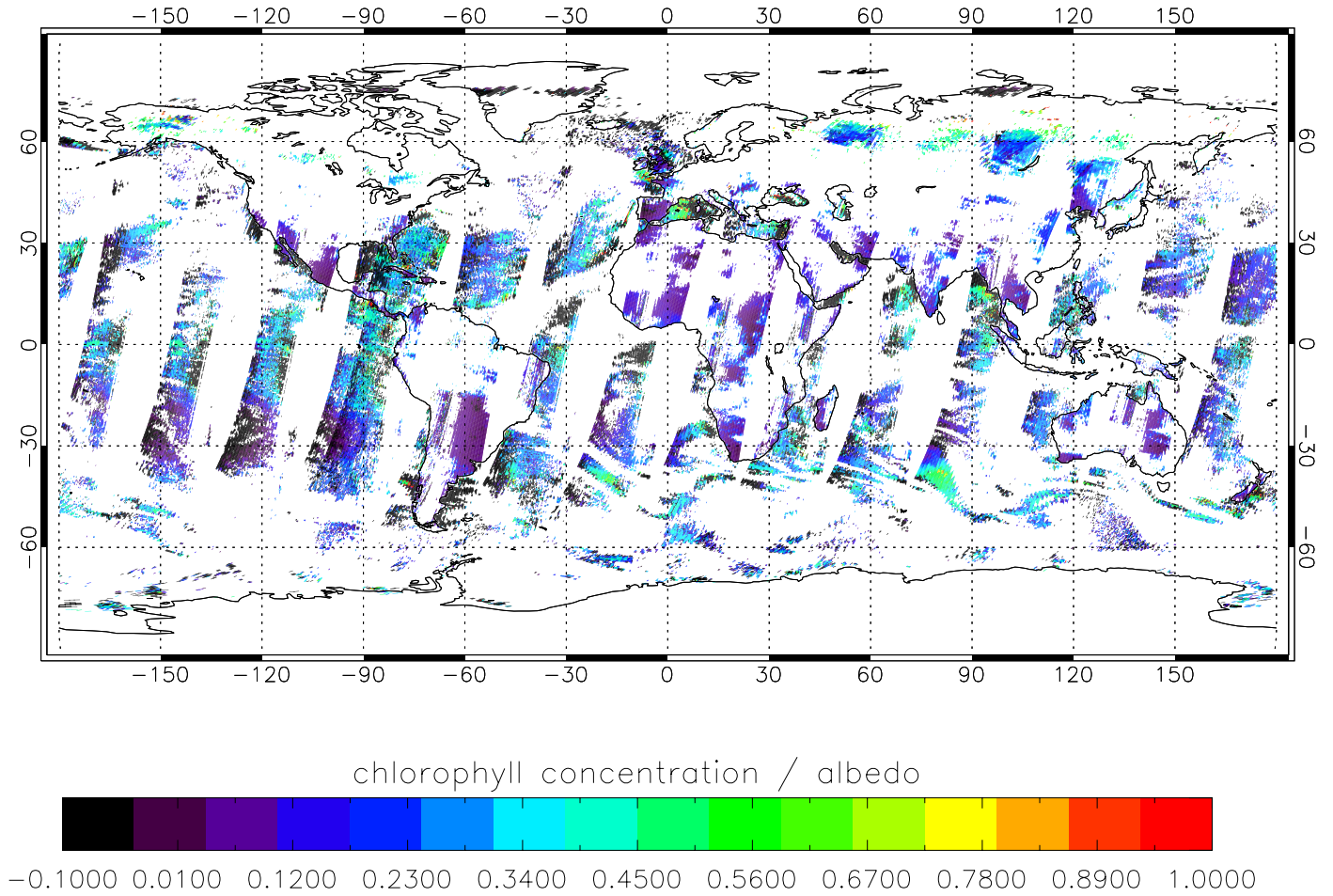


Figure 5.8: Retrieved chlorophyll concentration (ocean) and UV surface albedo (land) for 2008-02-05 for all scenes over the ocean that are selected as cloud-free

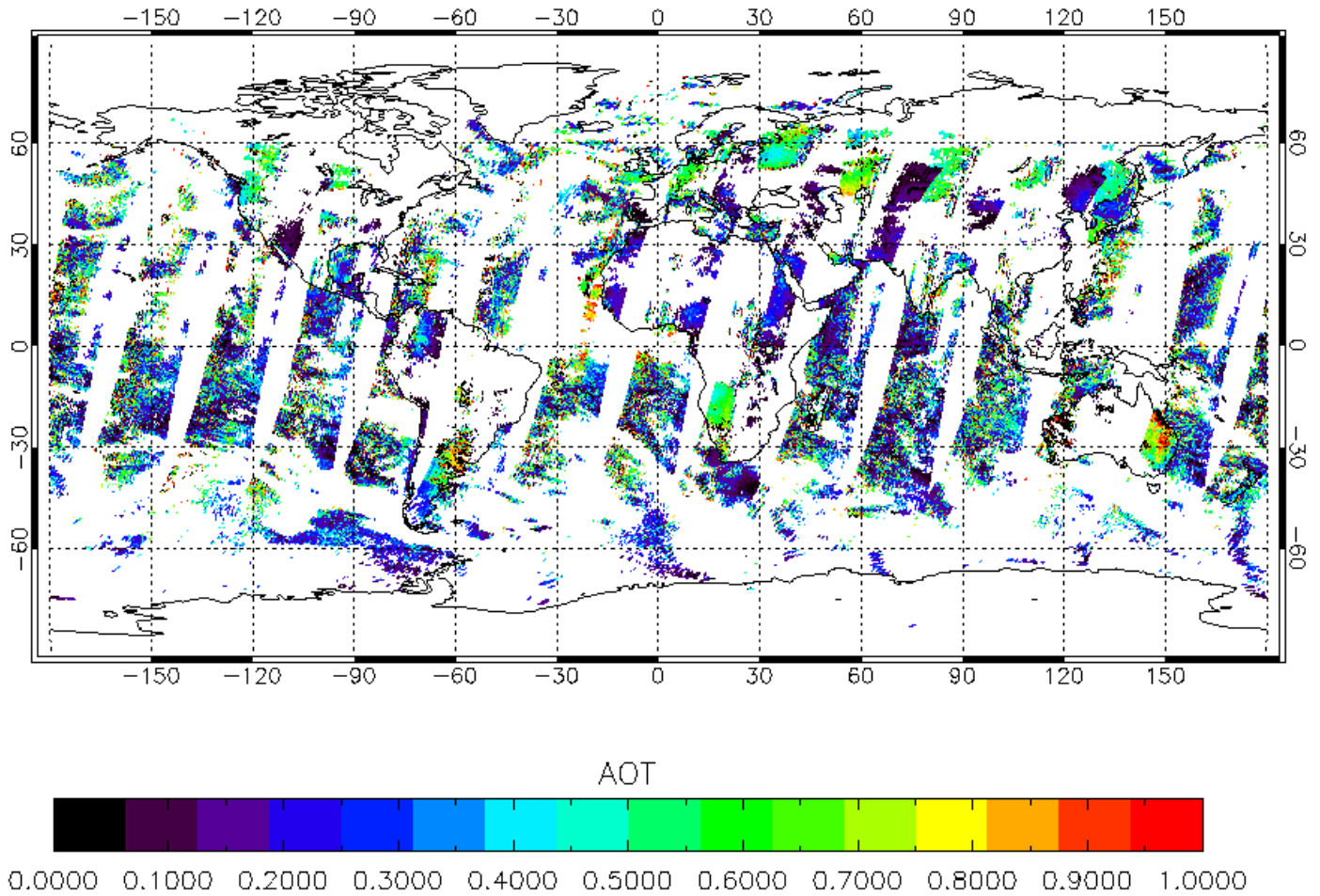


Figure 5.9: Retrieved AOT for 2008-04-01 for all scenes that are selected as cloud-free

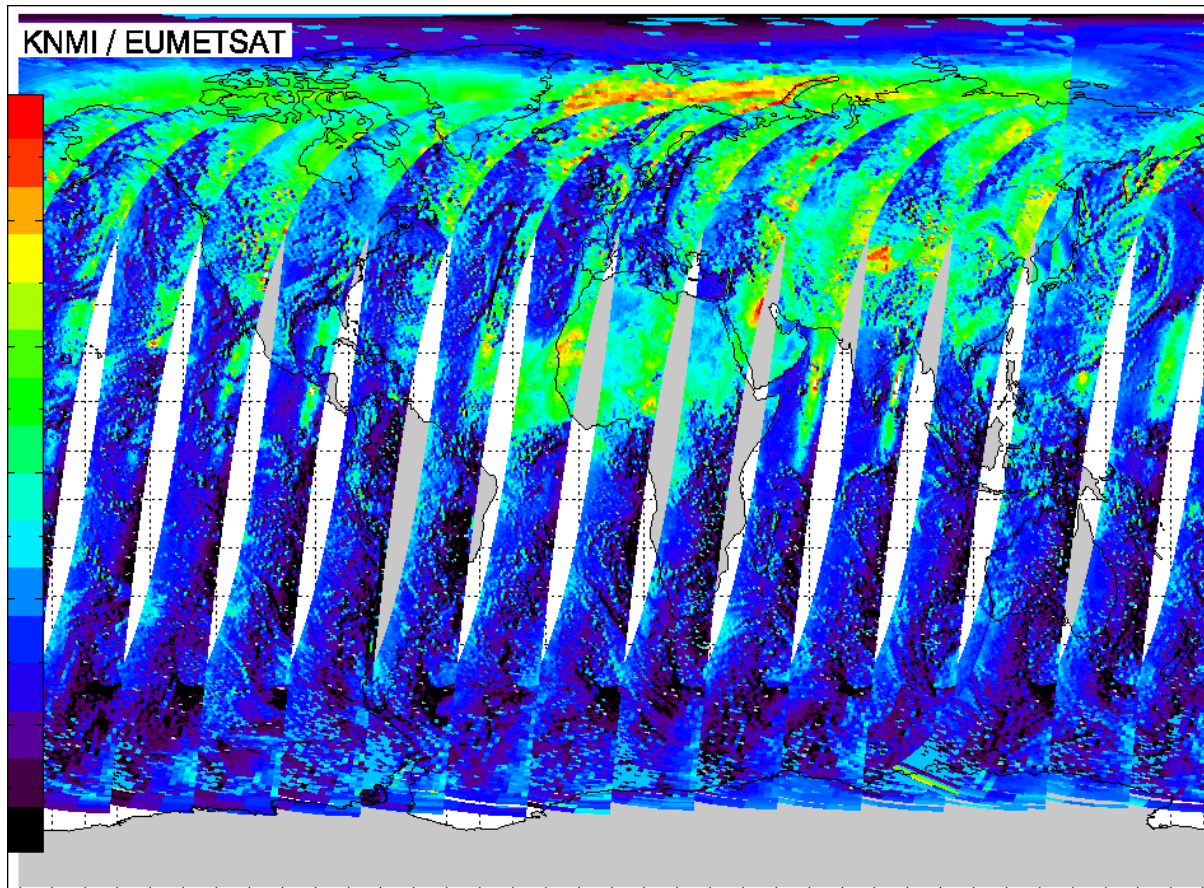


Figure 5.10: Aerosol Absorbing Index [de Graaf *et al.*, 2005] for GOME-2 data from 2008-4-01.

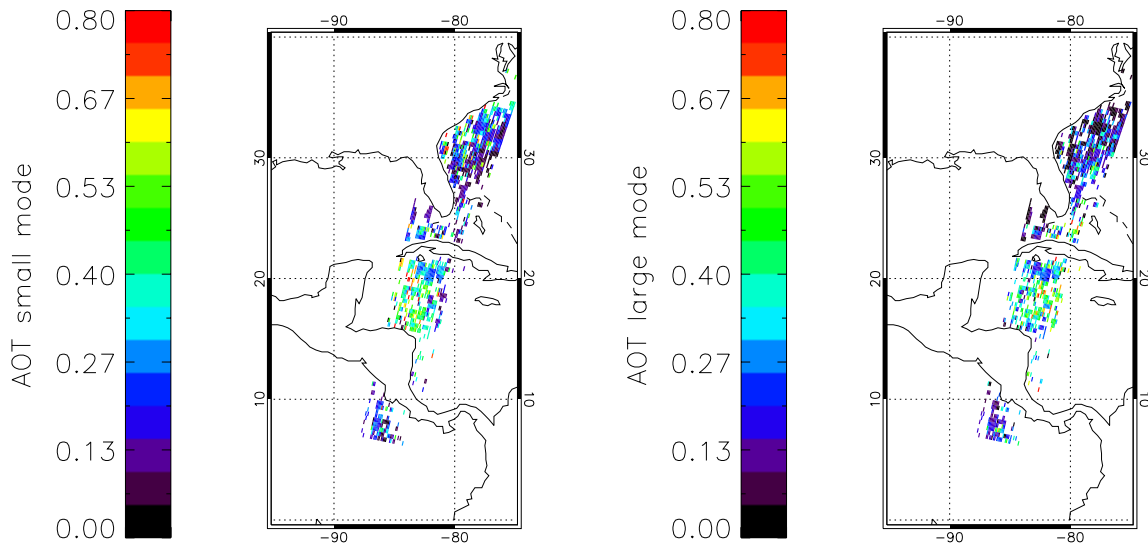


Figure 5.11: Aerosol optical thickness of the small mode (left) and of the large mode (right) retrieved by the full physics algorithm.

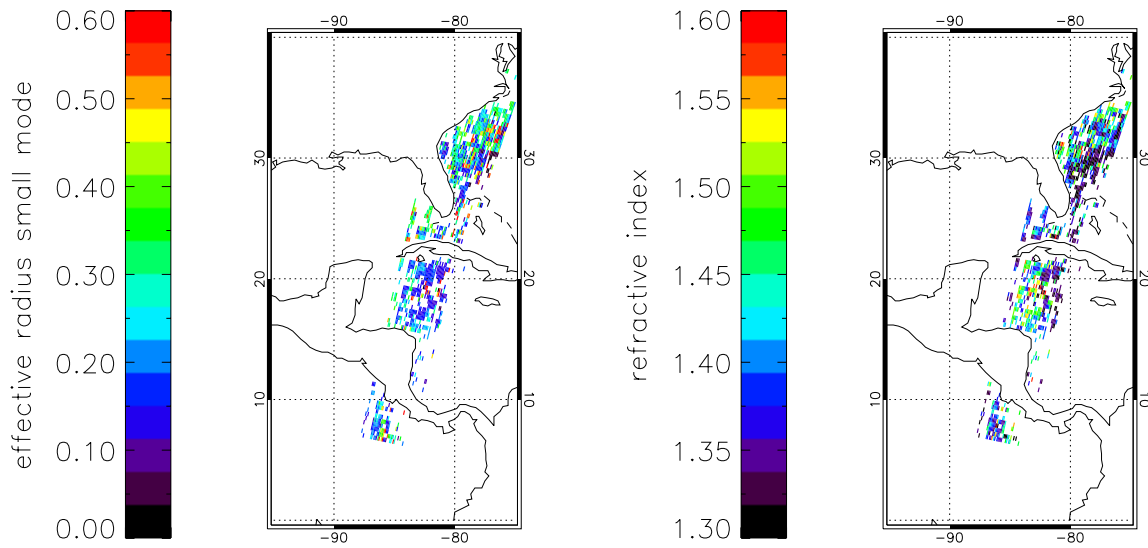


Figure 5.12: Effective radius of the small mode(left) and refractive index (right) retrieved by the full physics algorithm.

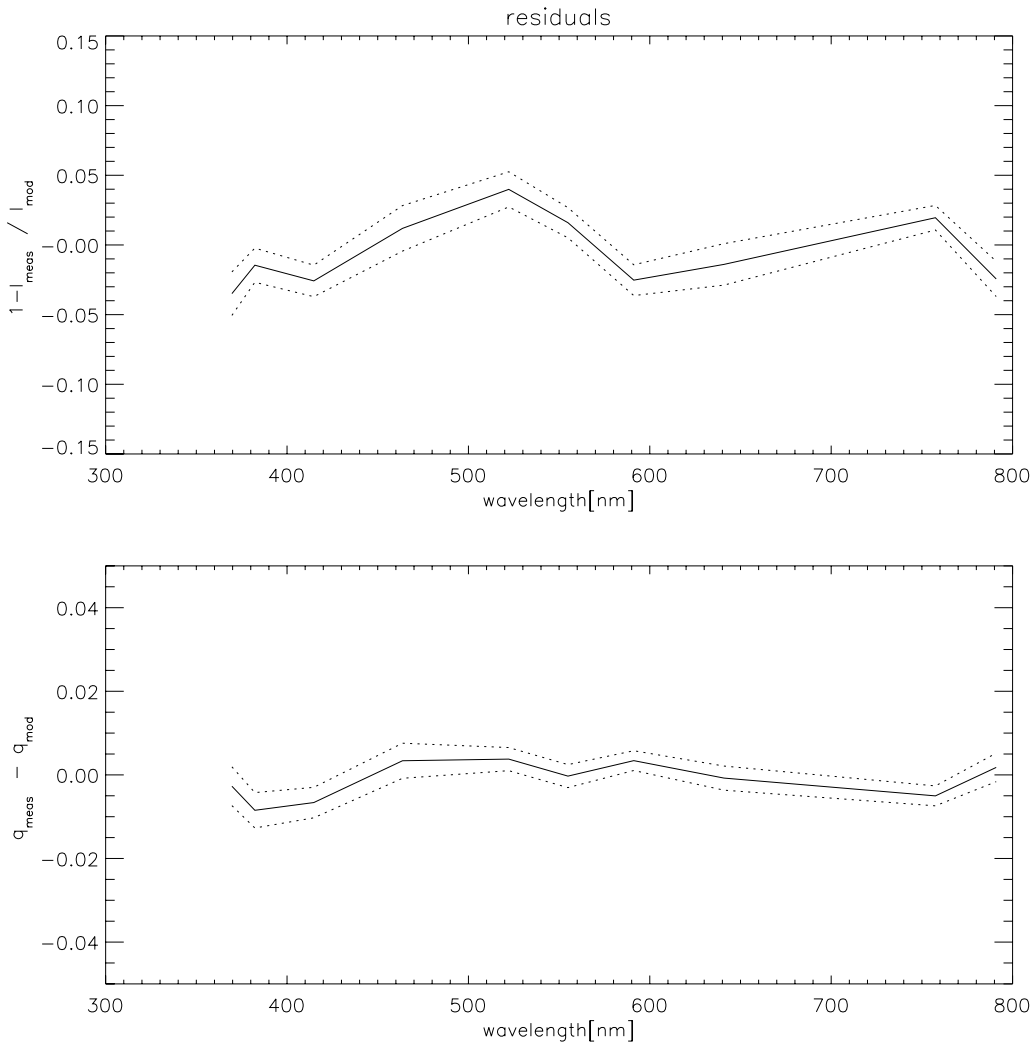


Figure 5.13: Mean residual and standard deviation of the fit between forward model and measurement for the total intensity I (upper panel) and Stokes fraction q (lower panel), for the data of Fig. 5.11.

index has different values here compared to other regions. Of course, an extensive validation of the parameters is required to investigate the quality of the retrievals. Here, a problem is that currently no other satellite instruments provide such detailed aerosol information as retrieved by the Full Physics Algorithm, and the availability of ground based measurements is limited for oceanic sites.

A first check for the quality of the retrieval is to evaluate how well the forward model calculations for the retrieved parameters agree with the measurement. Figure 5.13 shows the mean residual and standard deviation of the fit between forward model and measurement for the total intensity I and Stokes fraction q for all retrievals of Fig. 5.11. It can be seen that the mean residual in I show a strong variation with wavelength and is in the range -5-5 %. The standard deviation is in the range 1-2 %. Stokes fraction q is much better fitted, i.e. the mean residual is below 0.015 and the standard deviation is in the range 0.005-0.01. The fact that q is much better fitted than I is due to the fact that the calibration measurements of Stokes fraction q is improved based on measurements at geometries for which $\cos 2\chi = 0$. This re-calibration does not improve the accuracy of measurements of the total

intensity I . Therefore, it is needed to investigate possibilities to improve the quality of these measurements, for example by comparing them with the measurements of the GOME-2 main channels.

Chapter 6

Conclusions & Outlook

6.1 Conclusions

6.1.1 LUT-Based Algorithm

A fast algorithm for the retrieval of aerosol optical thickness has been developed. The algorithm is based on Lookup Tables of radiative transfer calculations for different aerosol models, different values of the AOT, and different surface reflection properties.

For aerosol retrieval over the ocean the measurements of Stokes parameters I and Q of all 10 PMD spectral bands between 369-791 nm are used. The retrieved parameters are the aerosol column integrated number density (directly related to the AOT) and the oceanic pigment concentrations. For the retrieval 29 aerosol models are used, where the model that fits best to the measurement is selected.

For aerosol retrieval over land only measurements are used that show small sensitivity to surface reflection properties. These are the measurements of the intensity of the PMD bands in the range 369-463 nm, and measurements of Stokes parameter Q of the PMD bands in the range 369-791 nm. For these retrievals we retrieve the column integrated number density and a spectrally independent Lambertian surface albedo for the range 369-791 nm. The reduced measurement vector for retrievals over land has a smaller sensitivity to aerosol microphysical properties than the measurement vector for retrieval over the ocean. Therefore, for retrievals over land a limited number of 6 aerosol models is used.

The algorithm has been applied to GOME-2 data of two days. Before application of the algorithm, we applied a re-calibration of the measurements of Stokes parameter q , using geometries for which $q = 0$, independent of atmospheric and surface properties [Aben *et al.*, 2003]. Also, we developed a cloud filter to select cloud free scenes. For retrievals over the ocean the cloud filter selects scenes with a large spectral contrast and a reflectivity in the red part of the spectrum smaller than a given threshold. For retrievals over land the selection is based only on a reflectivity threshold in the blue part of the spectrum.

In general, the retrieved AOT over the ocean is in the range that might be expected (0.1-0.3), although the mean AOT of 0.33 seems rather high. This may be due to insufficient cloud filtering. Some regions with enhanced aerosol are detected (Asia, Sahara). The enhanced values of the AOT west of the Sahara are qualitatively confirmed by the Aerosol Absorption Index deduced from GOME-2 main channel measurements. The aerosol models that best fit the measurement do in many cases not represent the expected aerosol types. This may be caused by the fact that it is not possible to describe the large range in microphysical aerosol parameters by a limited number of standard models. Another possible explanation would be the limited quality of the PMD level 1b measurements.

Over land the values appear to be too high and the results show unrealistic land-sea boundaries. Also, clear differences are seen between overlapping orbits. Clearly, the retrievals over land are subject to large uncertainties. This is caused (among other reasons) by the smaller information content caused by the reduced spectral range, the assumption that the surface is a Lambertian reflector, the stronger dependence on absolute calibration (not Stokes fraction q is used but Stokes parameter Q).

6.1.2 Full Physics Algorithm

A LUT based retrieval approach does not make full use of the increased information content of combined intensity and polarization measurements compared to instruments that measure only intensity. Namely, the additional use of GOME-2 polarization measurements allows the retrieval of information on size distribution and refractive index, which are essential parameters for climate research. In the paper of *Hasekamp and Landgraf* [2005b] a retrieval method is described that makes full use of the retrieval capabilities of GOME-2. In order to apply this approach to real data some adjustments of the algorithm had to be made.

The following parameters of a bi-modal aerosol model are retrieved: the height integrated aerosol number concentration of both modes, the effective radius of the small mode, the real part of refractive index, and the oceanic pigment concentration. It is confirmed by the study of *Hasekamp and Landgraf* [2005b] that GOME-2 measurements are most sensitive to this subset of parameters. These parameters are retrieved by least square fitting of a radiative transfer model to the GOME-2 measurements. In order to treat non-linearity we employ the Levenberg-Marquardt method [*Levenberg*, 1944; *Marquardt*, 1963]. For a sensitivity study and error analysis concerning the retrieval of microphysical properties, we refer to the paper of *Hasekamp and Landgraf* [2005b] and the O3MSAF Visiting Scientist report of *Hasekamp et al.* [2004]; *Hasekamp* [2005].

The Full Physics algorithm has been applied to a small set of GOME-2 data. The retrieved parameters are in the range that is physically expected. An extensive validation of the parameters is required to investigate the quality of the retrievals. Here, a problem is that currently no other satellite instruments provide such detailed aerosol information as retrieved by the Full Physics Algorithm, and the availability of ground based measurements is limited for oceanic sites. The fit between forward model and measurements is reasonably good (residuals in the range 0.005-0.015) for Stokes parameter q but are large (-5-5 %) for the total intensity I . This confirms on one hand the improved accuracy due to the re-calibration of q , but on the other hand it shows that the calibration of the PMD reflectance measurements needs to be improved.

6.2 Outlook

A major problem for aerosol retrieval from satellite measurements is cloud contamination. The GOME-2 retrievals described in this report make use of a simple cloud detection algorithm based on threshold on the spectral contrast and/or the reflectivity level. The values for the thresholds are rather arbitrary and therefore the cloud filter will not work properly in all situations: i.e. some cloud free pixels will be flagged as cloudy and vice versa. Therefore, an important recommendation for future work is to improve the detection of cloud free scenes. A possibility for improved cloud filtering is to treat clouds as a special type of aerosol with a specific size distribution and refractive index. The cloud optical thickness can then be retrieved in the same way as the AOT. It may be expected that the use of polarization allows for such a cloud detection approach, because of the high sensitivity of polarization measurements to particle size distribution and refractive index. Another possibility is to base a cloud filter on high spatial resolution measurements of the Advanced High Resolution Radiometer (AVHRR), that also flies on the METOP satellite. Further recommendations for future work include the verification and validation of the retrieval results, improvement of the calibration of the total intensity (and to a lesser extend of Stokes fraction q , and the improvement of the forward model, e.g. extension of the description of underwater scattering, and the inclusion of non-spherical aerosol particles in the retrieval algorithm.

Bibliography

- Aben, I., C. P. Tanzi, W. Hartmann, D. M. Stam, and P. Stammes, Validation of Space-Based Polarization Measurements by Use of a Single-Scattering Approximation, with Application to the Global Ozone Monitoring Experiment, *Appl. Opt.*, *42*, 3610–3619, 2003.
- Anderson, G. P., S. A. Clough, F. X. Kneizys, J. H. Chetwynd, and E. P. Shettle, Aflgl atmospheric constituent profiles (0-120 km), *AFGL Tech. Rep. AFGL-TR-86-0110*, Air Force Geophysical Laboratory, Air Force Base, Massachusetts, 1987.
- Callies, J., E. Corpaccioli, M. Eisinger, A. Hahne, and A. Lefebvre, GOME-2 - Metop's second-generation sensor for operational ozone monitoring., *ESA BULL-EUR SPACE*, *102*, 28–36, 2000.
- Chandrasekhar, S., *Radiative transfer*, Dover Publications, Inc., New York, 1960.
- Chowdhary, J., Multiple scattering of polarized light in atmosphere-ocean systems: Application to sensitivity analyses of aerosol polarimetry, Ph.D. thesis, Columbia University, 1999.
- Chowdhary, J., B. Cairns, M. Mishchenko, and L. Travis, Retrieval of aerosol properties over the ocean using multi-spectral and multiangle photopolarimetric measurements from the Research Scanning Polarimeter, *Geophys. Res. Let.*, *28*, 243–246, 2001.
- Chowdhary, J., B. Cairns, and L. Travis, Case studies of aerosol retrieval over the ocean from multiangle, multi-spectral photopolarimetric remote sensing data, *J. Atmos. Sci.*, *59*(3), 383–397, 2002.
- Chowdhary, J., B. Cairns, M. Mishchenko, P. Hobbs, G. Cota, J. Redemann, K. Rutledge, B. Holben, and E. Russel, Retrieval of aerosol scattering and absorption properties from photo-polarimetric observations over the ocean during the clams experiment, *J. Atmos. Sci.*, *62*(4), 1093–1117, 2005.
- Cox, C., and W. Munk, Statistics of the sea surface derived from sun glitter, *J. Mar. Res.*, *13*, 198–227, 1954.
- de Graaf, M., P. Stammes, O. Torres, and R. B. A. Koelemeijer, Absorbing Aerosol Index: Sensitivity analysis, application to GOME and comparison with TOMS, *Journal of Geophysical Research (Atmospheres)*, *110*, 1201–+, doi:10.1029/2004JD005178, 2005.
- Frouin, R., M. Schwindling, and P. Deschamps, Spectral reflectance of sea foam in the visible and near-infrared: In situ measurements and remote sensing implications, *J. Geophys. Res.*, *101*, 14,361–14,371, 1996.
- Hansen, J. E., and L. D. Travis, Light scattering in planetary atmospheres, *Space Sci. Rev.*, *16*, 527–610, 1974.
- Hasekamp, O., Algorithm development for aerosol retrieval over the ocean, *O3m-saf visiting scientist report*, EUMETSAT, 2005.

- Hasekamp, O., Feasibility study for aerosol retrieval over land, *O3m-saf visiting scientist report*, EUMETSAT, 2007.
- Hasekamp, O., and J. Landgraf, A linearized vector radiative transfer model for atmospheric trace gas retrieval, *J. Quant. Spectrosc. Radiat. Transfer*, 75, 221–238, 2002.
- Hasekamp, O., and J. Landgraf, Linearization of vector radiative transfer by means of the forward-adjoint perturbation theory and its use in atmospheric remote sensing, in *Light Scattering Reviews 2*, vol. 2, edited by A. Kokhanovsky, pp. 159–201, Springer, Berlin, 2007.
- Hasekamp, O., J. Landgraf, and R. van Oss, Aerosol retrieval studies for gome-2, *O3m-saf visiting scientist report*, EUMETSAT, 2004.
- Hasekamp, O. P., and J. Landgraf, Linearization of vector radiative transfer with respect to aerosol properties and its use in satellite remote sensing, *Journal of Geophysical Research (Atmospheres)*, 110, 4203–+, 2005a.
- Hasekamp, O. P., and J. Landgraf, Retrieval of aerosol properties over the ocean from multispectral single-viewing-angle measurements of intensity and polarization: Retrieval approach, information content, and sensitivity study, *Journal of Geophysical Research (Atmospheres)*, 110, 20,207–+, doi:10.1029/2005JD006212, 2005b.
- Koepke, P., and M. Hess, Scattering functions of tropospheric aerosols: The effect of nonspherical particles, *Appl. Opt.*, 27, 2422–2430, 1988.
- Kokhanovsky, A. A., Optical properties of irregularly shaped particles, *Journal of Physics D Applied Physics*, 36, 915–923, 2003.
- Kokhanovsky, A. A., Spectral reflectance of whitecaps, *Journal of Geophysical Research (Oceans)*, pp. 5021–+, 2004.
- Krijger, J. M., I. Aben, and H. Schrijver, Distinction between clouds and ice/snow covered surfaces in the identification of cloud-free observations using SCIAMACHY PMDs, *Atmospheric Chemistry & Physics*, 5, 2729–2738, 2005.
- Landgraf, J., O. Hasekamp, T. Trautmann, and M. Box, A linearized radiative transfer model for ozone profile retrieval using the analytical forward-adjoint perturbation theory, *J. Geophys. Res.*, 106, 27,291–27,306, 2001.
- Levenberg, K., A method for the solution of certain problems in least squares, *Quart. Appl. Math.*, 2, 164–168, 1944.
- Marquardt, D., An algorithm for least squares estimation of nonlinear parameters, *SIAM J. Appl. Math.*, 11, 431–441, 1963.
- Mishchenko, M., and L. Travis, Light scattering by polydispersions of randomly oriented spheroids with sizes comparable to wavelengths of observation, *Appl. Opt.*, 33, 7206–7225, 1994.
- Mishchenko, M., I. Geogdzhayev, B. Cairns, W. Rossow, and A. Lacis, Aerosol retrievals over the ocean by use of channels 1 and 2 AVHRR data: sensitivity analysis and preliminary results, *Appl. Opt.*, 36, 7325–7341, 1999.
- Mishchenko, M. I., and L. D. Travis, Satellite retrieval of aerosol properties over the ocean using polarization as well as intensity of reflected sunlight, *J. Geophys. Res.*, 102, 16,989–17,013, 1997a.

- Mishchenko, M. I., and L. D. Travis, Satellite retrieval of aerosol properties over the ocean using measurements of reflected sunlight, *J. Geophys. Res.*, *102*, 13,543–13,553, 1997b.
- Mishchenko, M. I., A. A. Lacis, B. Carlson, and L. Travis, Nonsphericity of dust-like tropospheric aerosols: Implications for aerosol remote sensing and climate modeling, *Geophys. Res. Lett.*, *22*, 1077–1980, 1995.
- Monahan, E., and I. O’Muircheartaigh, Optical power law description of oceanic whitecap coverage dependence on windspeed, *J. Phys. Oceanogr.*, *10*, 2094, 1980.
- Morel, A., Optical modeling of the upper ocean in relation to its biogenous matter content (case I waters), *J. Geophys. Res.*, *93*, 10,749–10,768, 1988.
- Morel, A., and B. Gentili, Diffuse reflectance of oceanic waters. II. Bidirectional effects, *Appl. Opt.*, *32*, 6864–6879, 1993.
- Morel, A., and L. Prieur, An analysis of variations in ocean color, *Limnol. Oceanogr.*, *19*, 591–600, 1977.
- Smith, R., and K. Baker, Optical properties of the clearest natural waters, *Appl. Opt.*, *20*, 177–184, 1981.
- Tanré, D., Y. Kaufman, M. Herman, and S. Mattoo, Remote sensing of aerosol properties over the ocean using the MODIS/EOS spectral radiances, *J. Geophys. Res.*, *102*, 16,971–16–988, 1999.
- Torres, O., R. Decaie, P. Veefkind, and G. de Leeuw, Omi aerosol retrieval algorithm, *ATBD-OMI-03*, pp. 47–69, 2001.
- Torricella, F., E. Cattani, M. Cervoni, R. Guzzi, and C. Levoni, Retrieval of aerosol properties over the ocean using Global Ozone Monitoring Experiment measurements: Method and application to test data, *J. Geophys. Res.*, *104*, 12,085–12,098, 1999.
- van de Hulst, H. C., *Light scattering by small particles*, J. Wiley and sons, New York, 1957.
- Veefkind, J., G. de Leeuw, P. Stammes, and R. Koelemeijer, Regional distribution of aerosols over land derived from ATSR-2 and GOME, *Remote Sens. Env.*, *74*, 377–386, 2000.
- Wiscombe, W., and G. Grams, Scattering from nonspherical Chebyshev particles,2, Means of angular scattering patterns., *Appl. Opt.*, *27*, 2405–2421, 1988.